ROYAL SOCIETY
OF CHEMISTRY

REVIEW

Check for updates

Recent progress of sulphur-containing high-efficiency organic light-emitting diodes (OLEDs)

Zijun Feng, Zhuang Cheng, Haixu Jin and Ping Lu (ID) *

In the last few decades, organic light-emitting diodes (OLEDs) have been rapidly developed and occupy an important position in the lighting and display market. Early conventional fluorescent OLED materials can only utilize 25% of excitons. Improving the harvest of non-emissive triplets has become the most important issue in this field. Organic electroluminescent materials have been developed from the first generation of fluorescent materials to the second generation of phosphorescent materials, and to the new generation of luminogens, mainly including triplet–triplet annihilation (TTA) materials, thermally activated delayed fluorescence (TADF) materials and hot exciton materials. The new generation of luminogens is mainly constructed using heterocyclic compounds with a D–A structure. Sulphur-fused heterocyclic derivatives are some of the most investigated heterocyclic compounds. Sulphur possesses two lone pairs of electrons and an empty d orbital with an outermost electron structure of $3s^2 3p^4$. Sulfoxide or sulfone with electron-deficient characteristics can be easily formed by oxidation of sulphur, which is beneficial to electron injection and transportation. All these features make sulphur-fused heterocyclic derivatives an appealing building block for the new generation of luminogens. Herein, recent progress of efficient OLEDs based on sulphur-containing heterocyclic compounds, involving thiophene, phenylsulfone, thiazole and phenothiazine, as the active layers, is systematically summarized. The fundamental principles regarding molecular design are discussed, and representative reported TADF and hot exciton sulphur-based luminogens are summarized and analyzed, along with their structure–property relationships and OLED applications. As a structure/property/device performance relationship map is drawn, it is hoped that the review indicates one way to obtain better performance of this series of promising OLEDs.

1. Introduction

Since the pioneering work of organic light-emitting diodes (OLEDs) based on vacuum evaporation reported by Tang and

Van Slyke in 1987, OLEDs have exhibited promising prospects and aroused extensive attention.[1] In the past few decades, OLEDs have been gradually developed and occupy an important position in the lighting and display market, owing to their advantages of self-illumination, high brightness, fast response, flexibility being easy to process, *etc.*[2,3] According to the spin statistical theory, electrically excited electrons would produce

State Key Laboratory of Supramolecular Structure and Materials, Jilin University, Qianjin Street No. 2699, Changchun, 130012, P. R. China. E-mail: lup@jlu.edu.cn

Zijun Feng received his bachelor's degree in Chemistry from Jilin University in 2019. He is now a PhD candidate at the State Key Laboratory of Supramolecular Structure and Materials, College of Chemistry, Jilin University. His research interest is focused on light-emitting materials of organic light-emitting diodes.

Zijun Feng

Zhuang Cheng received his bachelor's degree in Chemistry from Jilin University in 2020. He is now a master's degree candidate at the State Key Laboratory of Supramolecular Structure and Materials, College of Chemistry, Jilin University. His current scientific interest is focused on the device physics of organic light-emitting materials and devices.

Zhuang Cheng

25% singlet excitons and 75% triplet excitons, and only the singlet excitons can be utilized for fluorescence, which results in a limited internal quantum efficiency (IQE) of up to 25% for the first-generation of luminescent materials. Moreover, with an out-coupling efficiency of 20%, the maximum external quantum efficiency (EQE) is only 5%, which is too low to put into practical application.[4] To utilize non-emissive triplet excitons, heavy-metal atoms were introduced and coordinated with organic molecules, which facilitates phosphorescence emission in OLEDs.[5–10] Since the ISC process can be significantly improved by heavy-metal atoms by enhancing the spin orbital coupling (SOC) effect, the second-generation of phosphorescent OLED (PHOLED) materials could achieve a theoretical maximum IQE of 100%.[11] Although the PHOLEDs with an excellent maximum EQE spring up like mushrooms, there are still core issues that need to be addressed: the extremely serious triplet–triplet annihilation (TTA) effect under high operating current density, high preparation cost, and deficient device lifetime.[12] In recent years, a great deal of endeavors have been devoted to the OLEDs based on pure organic small molecules which can utilize triplet excitons. The main mechanisms for harvesting triplet energy include TTA,[13–15] hot excitons,[16–18] and thermally activated delayed fluorescence (TADF).[19,20] TTA is a characteristic mechanism to up-convert the triplet excited states with low energy into singlet excited states (Fig. 1). To accomplish this up-conversion process, two excited T excitons generate one excited S exciton and one exciton in the ground state by a fusion and RISC process. Jortner et al.[21] proposed that when two triplet excitons are annihilated to generate an intermediate state ($(TT)^{**}$), there is a 1/9 probability that they would form a singlet intermediate state ($^1(TT)^{**}$), 3/9 probability that they would form a triplet intermediate state ($^3(TT)^{**}$), and 5/9 probability that they would generate a quintet intermediate state ($^5(TT)^{**}$). $^1(TT)^{**}$ can be converted to S_1 and S_0, $^3(TT)^{**}$ can be converted to T_1 and S_0, and $^5(TT)^{**}$ can be converted to T_1 and S_0 or two T_1. Theoretically, when all the intermediate states are transformed into singlet excitons during the TTA process, the total IQE can reach 62.5% with an up-conversion efficiency of 50%. Furthermore, assume
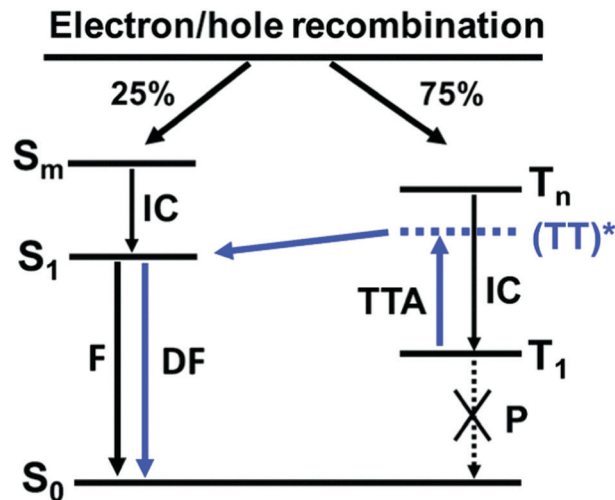

Fig. 1 Photophysical mechanism of TTA.

that the devices' optical out-coupling is 20%, the maximum EQE of devices based on the TTA mechanism could reach 12.5%, and this is a significant improvement over the 5% EQE of traditional fluorescent OLEDs.[22]

However, an EQE of 12.5% is not enough to satisfy the demand for higher device performance. Hence, tremendous efforts have been devoted to TADF emitters, which theoretically could achieve a maximum IQE of 100% (Fig. 2). The key luminescence mechanism of TADF is as follows: under the premise that the exchange energy (ΔE_{ST}) between the lowest triplet excited state (T_1) and the lowest singlet excited state (S_1) is small enough, the T_1 state flips to the S_1 state through the reverse intersystem crossing (RISC) phenomenon at room temperature, and then the S_1 state emits delayed fluorescence through the radiation transition.[23] Therefore, a TADF emitter can be achieved by designing molecules with twisted geometries in which the spatial overlap between the highest occupied molecular orbital (HOMO) level and lowest unoccupied molecular orbital (LUMO) level is small enough to result in a small ΔE_{ST} because

Haixu Jin received his bachelor's degree in Chemistry from Zhengzhou University in 2019. He is now a master's degree candidate at the State Key Laboratory of Supramolecular Structure and Materials, College of Chemistry, Jilin University. His current scientific interest is ed on blue organic light-emitting materials and devices.

Haixu Jin

Ping Lu received her PhD degree in polymer chemistry and physics from Jilin University in 2005. And then, she joined the State Key Lab of Supramolecular Structure and Materials, Jilin University. She worked as a postdoctoral research fellow at the Hong Kong University of Science and Technology from 2009 to 2010. She was promoted to be a full professor in 2014 at Jilin University. Her current research interests are focused on organic/ polymer optoelectronic materials and devices.
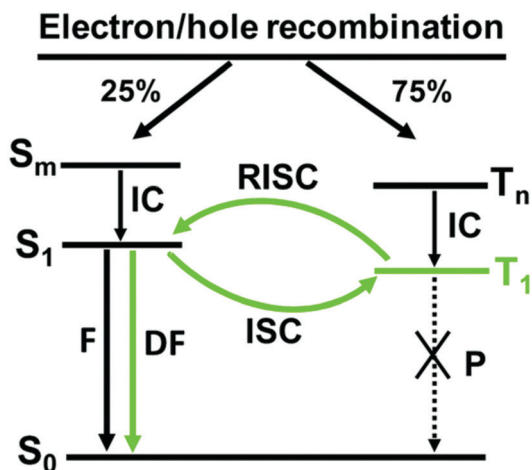
Ping Lu

4498 | *J. Mater. Chem. C*, 2022, **10**, 4497–4520

This journal is © The Royal Society of Chemistry 2022

Fig. 2 Photophysical mechanism of typical TADF.

Fig. 4 Electron structure, type of hybridization and bonding in S atoms.

the interchange interaction integral of ΔE_{ST} and the spatial wave function between the frontier molecular orbitals (FMOs) is inversely proportional.[24]

However, TADF-based OLEDs encounter serious roll-offs or unsatisfactory operation lifetimes of devices caused by the long triplet lifetime. Different from TADF, triplet excitons can be harvested by the conversion process from triplet states T_n ($n \geq 2$) to singlet states S_m ($m \geq 1$), which is named the "hot exciton" process (Fig. 3). The hot exciton mechanism allows RISC to occur between the singlet and triplet excited states at higher energy levels, which enables a high efficiency and short triplet excited state lifetime to be achieved simultaneously.[25] In early studies, it was found that RISC from higher triplet states (hRISC) exists in organic molecules such as naphthalene, quinoline, isoquinoline, fluorene, rose bengal, tetraphenylporphyrin, cyanine dyes, anthracene and its derivatives, and some excited-state intramolecular proton transfer (ESIPT) materials.[26–31] Nowadays, this photophysical phenomenon is applied in organic electroluminescence (EL), and triplet exciton-utilized OLEDs with
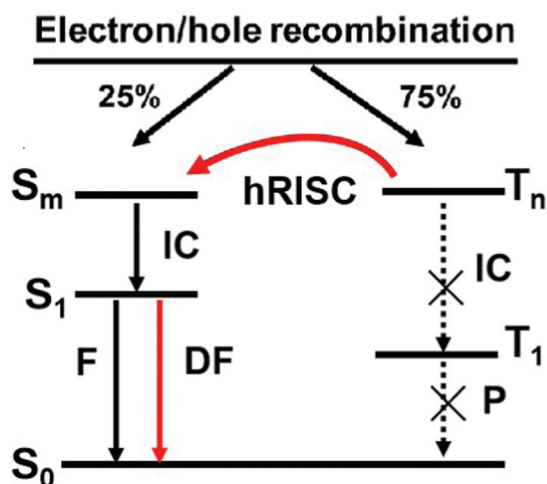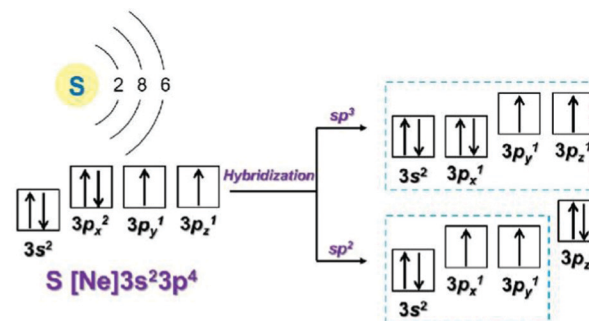
high efficiency and various colors have been successfully obtained.[14,32–36]

Sulfur lies in the second row of the periodic table and belongs to the oxygen family, with an outermost electron structure of $3s^23p^4$ and an empty d orbital (Fig. 4). A sulfur-containing molecule is a kind of sparkling structure in chemistry, which is put into a plethora of applications ranging from medicine to optics and nanotechnology to separation science.[37] For applications in OLEDs, sulphur-fused heterocyclic derivatives represent one of the most investigated heterocyclic compounds. Sulfoxide or sulfone with electron-deficient characteristics can be easily formed by oxidation of sulphur, which is beneficial to electron injection and transportation. These sulphur-fused heterocyclic derivatives are commonly used as host materials or emissive layers in OLEDs.[38–40] It is also easy to substitute sulphur atoms with selenium or tellurium, heavy atoms in the same main group, through typical replacement reactions, which greatly reduces the LUMO energy level and red-shifts the emission spectra. Compared with O atoms, S atoms in organic molecules are more likely to lead to a distorted spatial geometry, which is attributed to its larger atomic radius (extra electron orbitals).[41]

Research studies of efficient sulphur-containing chromophores have been carried out for a long time, and reports of these emitters are mainly based on dibenzothiophene (**DBT**), diphenyl sulfone (**DPS**), thiadiazole (**BZ/NZ**), and phenothiazine (**PTZ**). Herein, a review of the recent progress in the above heterocyclic emitters is presented. The fundamental principles regarding molecular design are discussed, and representative reported TADF and hot exciton sulphur-based luminogens are summarized and analyzed, along with their structure–property relationships and OLED applications. By summarizing these efficient emitters with sulphur-containing chromophores, we expect to provide serviceable design strategies to deliver more efficient sulphur-containing compounds with high OLED performance.

2. High-efficiency emitters based on S-containing chromophores

In this paper, emitters based on the following four derivatives containing S chromophores are discussed: **DBT** with a rigid structure, **DPS** with an electron-withdrawing capacity, **BZ/NZ**

Fig. 3 Photophysical mechanism of hRISC.

with a flat structure and electron-withdrawing capacity, and **PTZ** with multiple distorted conformations caused by the large diameter of S atoms.

2.1 DBT based emitters

DBT possesses a rigid structure. The sulphur atom in **DBT** undergoes sp^3 unequal hybridization with two lone pairs of electrons, which usually serves as an electron-rich donor. In the early research of OLEDs, **DBT** is often used in polymer light-emitting diodes (PLEDs) owing to its good hole-transporting properties.[42–44] Recently, **DBT** has also been applied to synthesize TADF materials.

In 2017, Tang and co-workers reported a TADF-AIE (aggregation-induced emission)-ML (mechanoluminescence) emitter, **DBT-BZ-DMAC** (Fig. 5).[45] **DBT-BZ-DMAC** had an unsymmetrical D–A–D′ structure, where benzoyl (**BZ**) served as an electron acceptor, and 9,9-dimethyl-9,10-dihydroacridine (**DMAC**) and **DBT** functioned as electron donors (D and D′, respectively). The **DMAC** and **BZ** formed a twisted conformation to realize AIE and TADF properties, while the planar **DBT** helped to increase the charge-transporting ability of the luminogen. The crystal analysis of **DBT-BZ-DMAC** showed that the **BZ-DMAC** segments with charge transfer (CT) properties form hydrogen bonds between molecules to obtain a high photoluminescence (PL) efficiency and a small red-shift in the solid state (Fig. 6). The PL efficiency of the 4,4′-di(9H-carbazol-9-yl)-1,1′-biphenyl (CBP, Fig. 20) doped film is 65.9%, lower than the 80.2% PL efficiency of the **DBT-BZ-DMAC** pure film, indicating that **DBT-BZ-DMAC** did not need doping to prevent emission quenching due to its AIE nature. Doped and non-doped OLEDs were fabricated by adopting **DBT-BZ-DMAC** as the emitter. The doped OLEDs with a low doping concentration afforded superb peak EL efficiencies, but the efficiency roll-off remained large, like most doped OLEDs with TADF emitters in the literature. With the increase of doping concentration, the peak efficiency values were decreased but the efficiency roll-off apparently became smaller. The non-doped OLEDs provided excellent peak EL efficiencies of 43.3 cd A^{-1}, 35.7 lm W^{-1}, and 14.2%, with an extremely small current efficiency (CE) roll-off of 0.46%, and an external CE roll-off approaching null from peak values to those at 1000 cd m^{-2}, enabling non-doped OLEDs to
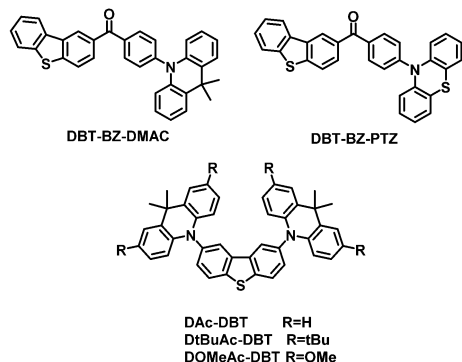

Fig. 5 Molecular structures of the materials used in Section 2.1.
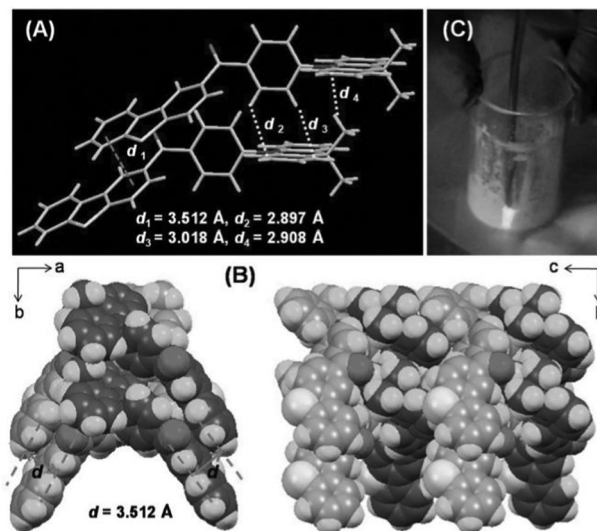

Fig. 6 (A and B) Packing patterns of **DBT-BZ-DMAC** in crystals. (C) Mechanoluminescence photo of the as-prepared **DBT-BZ-DMAC** crystalline powders, upon scratching under ambient conditions without UV illumination. Reproduced with permission from ref. 45. Copyright 2017 John Wiley & Sons.

outperform doped OLEDs at high luminance. In doped OLEDs of **DBT-BZ-DMAC** show high peak current and external quantum efficiencies of up to 51.7 cd A^{-1} and 17.9%, respectively, but the efficiency roll-off is large at high luminance. In the same year, Wang *et al.* calculated the quantum mechanics (QM) and molecular mechanics (MM) of **DBT-BZ-DMAC** and analyzed the XRD of its crystal and powder.[46] The results indicated that the non-radiative decay rate of **DBT-BZ-DMAC** in the solid phase was significantly decreased due to the suppression of the rotation of the **DMAC** and **DBT** units, while the radiative rate was greatly increased owing to the enhancement of the transition dipole moment. Both the intersystem crossing (ISC) and RISC processes happened between the S$_1$ and the lowest degenerate T$_1$ and T$_2$ states (Fig. 7). In addition, the CT rate was studied using the Marcus theory and the intrinsic charge mobility was calculated by performing the kinetic Monte Carlo method. The results showed that the **DBT-BZ-DMAC** crystal was a p-type semiconductor with a hole mobility of 0.14 cm^2 V^{-1} s^{-1} at room temperature.

In 2017, Tang *et al.* prepared two molecules, **DBT-BZ-PXZ** and **DBT-BZ-PTZ**, in which the planar **DBT** was used as the invariable donor to increase the charge-transporting ability of the materials. Phenoxazine (**PXZ**) and **PTZ** showed good electron-donating and hole-transporting abilities and promoted the separation of the HOMO and LUMO with a **BZ** acceptor.[47] Both OLED materials based on the two molecules exhibited TADF-AIE properties. For example, for X-ray crystallography of **DBT-BZ-PXZ**, the dihedral angle between the donor **PXZ** and benzene reached 66° (Fig. 8), which facilitated the HOMO/LUMO separation and made the molecules loosely stack in the crystal lattice. There was no tight π–π stacking between **DBT** and **BZ** fragments. Multiple C–H···π and C=O···H hydrogen bonds were also observed. The non-radiative decay was inhibited by

4500 | *J. Mater. Chem. C*, 2022, **10**, 4497–4520

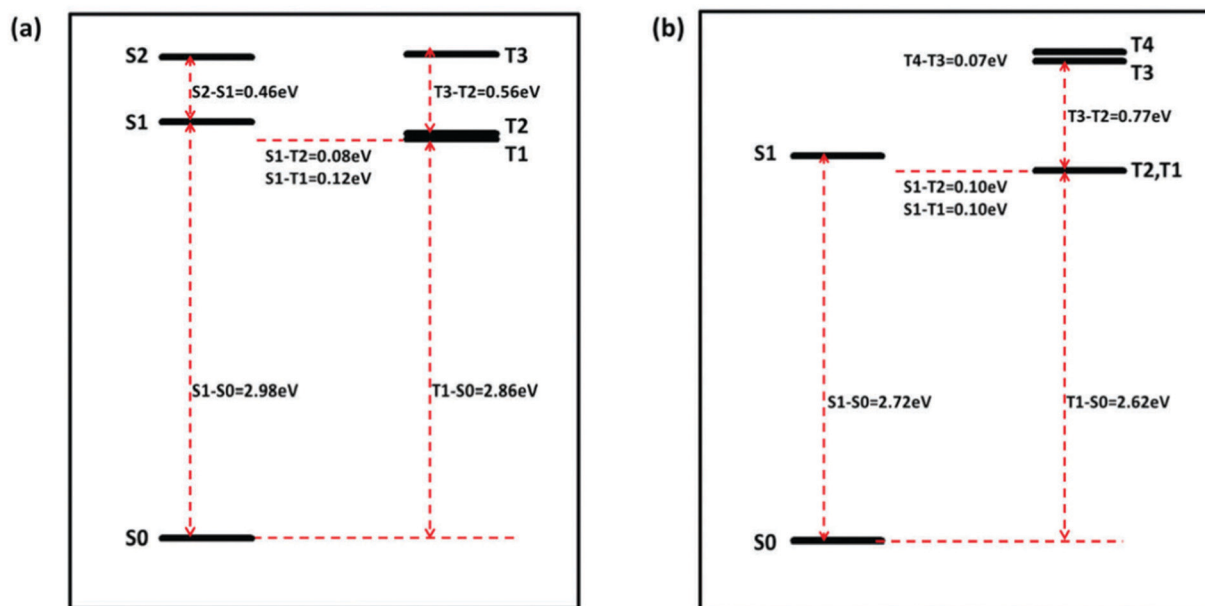This journal is © The Royal Society of Chemistry 2022

Fig. 7 Adiabatic excitation energies for **DBT-BZ-DMAC** in the gas (a) and solid phases (b), respectively.
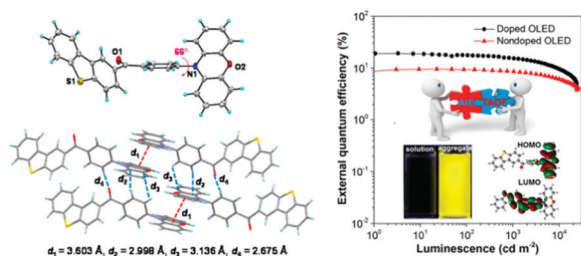

Fig. 8 Crystal structure (CCDC 1455106) and packing pattern of **DBT-BZ-PXZ** in crystals. Reproduced with permission from ref. 47. Copyright 2017 American Chemical Society.
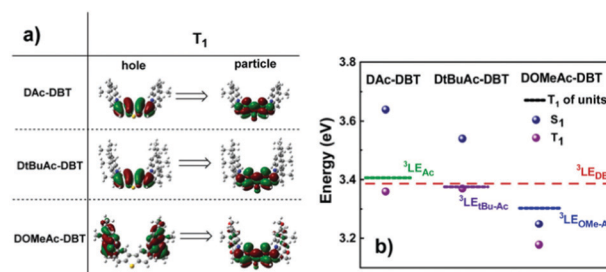

Fig. 9 (a) Natural transition orbitals (NTO) corresponding to the first triplet transitions. (b) Singlet and triplet energy diagrams of **DAc-DBT**, **DtBuAc-DBT** and **DOMeAc-DBT** along with the energy levels of the individual units (TD-DFT rBMK/6-31G(d)).

various intermolecular interactions and the luminescence efficiency of the concentrated state was improved. The maximum EQEs of the doped device based on **DBT-BZ-PXZ** and **DBT-BZ-PTZ** reached 15.1% and 19.2%, respectively. It is worth mentioning that the maximum EQE of non-doped devices based on **DBT-BZ-PTZ** was 9.7%, and the maximum EQE of 8.5% was still maintained under the brightness of 1000 cd m^{-2}. This work showed that the roll-off of undoped devices based on TADF-AIE materials could be significantly suppressed at high brightness.

The manipulation of the emission properties of deep-blue emitters with TADF features through molecular design is challenging. In 2019, Dias et al. synthesized three TADF molecules, **DAc-DBT**, **DtBuAc-DBT** and **DOMeAc-DBT**, applying **DBT** as an unconventional acceptor to fulfill this goal.[48] The design of **DAc-DBT** derivatives was inspired by a previously synthesized molecule, **DPTZ-DBT**,[49] which exhibited excellent room temperature phosphorescence (RTP) emission. In the tert-butyl substituted compound the low energy triplet was localized on the acceptor unit (Fig. 9), with the RISC mechanism ($k_{RISC} = 0.17 \times 10^5$ s^{-1}) likely involving the mixture of CT and locally excited (LE) triplet states that were varied by less than 0.09 eV. An optimized OLED based on the tBu-compound presented a maximum EQE of 10.5% and a deep-blue emission with CIE coordinates of (0.133, 0.129).

2.2 DPS-based emitters

DPS is widely used in blue light emitting materials with a D–A structure owing to its relatively shallow LUMO energy level and distorted spatial conformation. In recent years, **DPS** has been acting as a classical acceptor for blue TADF materials with excellent device performance.[50–52]

In 2012, Adachi's group published a paper on the synthesis of three blue TADF molecules **DPA-DPS**, **TDPA-DPS** and **TDTC-DPS** (Fig. 11) using **DPS** as the acceptor, and diphenylamine (**DPA**), di-tert-butyldiphenylamine (**TDPA**) and di-tert-butylcarbazole (**TDTC**) as the respective donors.[53] All three compounds exhibited broad and structureless emission bands with maxima between 402–419 nm, which could be ascribed to the intramolecular CT transition because of their dipolar nature.

This journal is © The Royal Society of Chemistry 2022

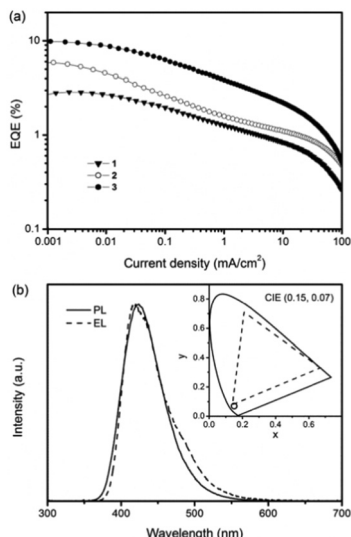J. Mater. Chem. C, 2022, **10**, 4497–4520 | **4501**

Fig. 10 (a) The EQE–current density characteristics of the OLEDs based on (1) **DPA-DPS**, (2) **TDPA-DPS** and (3) **TDTC-DPS**. (b) The EL and PL spectra of 10 wt% **TDTC-DPS** doped in a DPEPO layer. Inset: The CIE coordinates of the EL spectrum of a **TDTC-DPS**-based device. Reproduced with permission from ref. 53. Copyright 2012 American Chemical Society.

Their ΔE_{ST} values were calculated to be slightly raised for the ^{1}CT state, and considerably raised for the $^3\pi\pi^*$ state, 0.54, 0.45, and 0.32 eV, respectively. The introduction of *tert*-butyl groups on the **DPA** unit enhanced its electron donating ability, and consequently lowered the CT energy and the ΔE_{ST}. On the other hand,

the replacement of a **DPA** unit with a carbazole (**Cz**) unit slightly raised the ^{1}CT state, and considerably raised the $^3\pi\pi^*$ state, resulting in a further decrease in its ΔE_{ST}. **TDTC-DPS** based OLEDs achieved the best performance with a maximum EQE of 9.9% and EL peaking at 423 nm (Fig. 10). This was a very impressive device performance at the time, and opened a relatively simple and intuitive path for the manufacture of efficient blue TADF materials.

Subsequently, on the basis of **TDTC-DPS**, Adachi *et al.* replaced the *tert*-butyl group with a methoxyl group to produce a new compound **DMOC-DPS** (Fig. 11).[54] **DMOC-DPS** exhibited a much shorter excited-state lifetime in both aromatic solution and organic thin film, because the change of the substituent on the donor affected the S_1 and T_1 excited states in different ways, decreasing the energy gap between the S_1 and T_1 states. **DMOC-DPS** possessed a smaller ΔE_{ST} (0.24 eV) relative to that of **DTC-DPS** in organic thin films, because the change of the substituent on the donor affected the S_1 and T_1 excited states in different ways, decreasing the energy gap between the S_1 and T_1 states. **DMOC-DPS** possessed a smaller ΔE_{ST} (0.24 eV) relative to that of **DTC-DPS** in toluene (0.32 eV). OLEDs based on **DMOC-DPS** achieved a maximum EQE of 14.5% with an EL peak at 460 nm and CIE coordinates of (0.16, 0.16), which was the highest level of blue OLEDs at the time. In addition, it is worth noting that the roll-off of **DMOC-DPS** was reduced and there was still a 9.0% EQE at 100 cd m^{-2}. This work successfully provided an effective path for the design of low roll-off OLED materials.
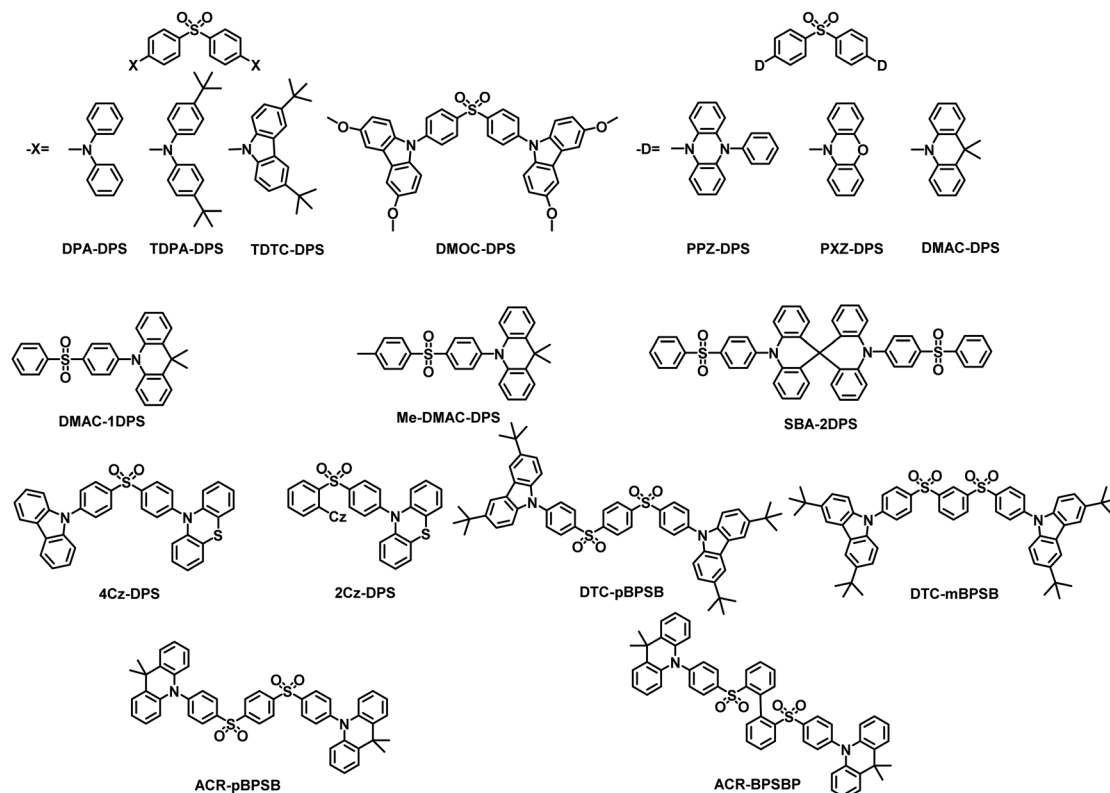

Fig. 11 Molecular structures of the materials containing **DPS** units.

4502 | *J. Mater. Chem. C*, 2022, **10**, 4497–4520

This journal is © The Royal Society of Chemistry 2022

Adachi and co-workers continued to explore the DPS-based blue TADF material. In 2014, they reported three TADF molecules, **PPZ-DPS**, **PXZ-DPS**, and **DMAC-DPS** (Fig. 11).[50] A relatively large torsion angle of 89° was obtained between **DMAC** and **DPS**. Such a large degree of distortion resulted in a small overlap between the HOMO and LUMO in **DMAC-DPS**, resulting in a ΔE_{ST} less than 0.1 eV. The non-doped device based on **DMAC-DPS** eventually achieved the CIE coordinates of (0.16, 0.20), an EL emission peak at 470 nm and a surprisingly high maximum EQE of 19.5%, representing one of the best device performances so far. The ΔE_{ST} was small enough to significantly suppress the roll-off, and the EQE still remained at 16.0% at 1000 cd m^{-2} brightness. This work provided valuable guidance for achieving efficient blue TADF materials.

In 2015, Adachi *et al.* further optimized the device structure of **DMAC-DPS** and prepared high-efficiency simple non-doped devices that could be as efficient as the best doped OLEDs.[55] A blue-emitting undoped OLED employing the **DMAC-DPS** derivative achieved an EQE of 19.5% at a luminescence of 100 cd m^{-2} (Fig. 12). It was found that a relatively large Stokes' shift and weak π–π stacking interactions were responsible for the concentration insensitive properties of the TADF emitter. This was another big advantage of TADF-based OLEDs compared with PHOLEDs.

In 2019, Yang *et al.* reported two TADF-AIE molecules **mono-DMACDPS** (**DMAC-1DPS**) and **Me-DMAC-DPS** (Fig. 11) with the goal of designing multifunctional organic emitters.[56] **mono-DMACDPS** and **Me-DMACDPS** exhibited typical AIE, TADF, and room temperature phosphorescence (RTP) properties but different ML behaviors. Crystal structure analysis revealed that a large dipole moment and multiple intermolecular interactions
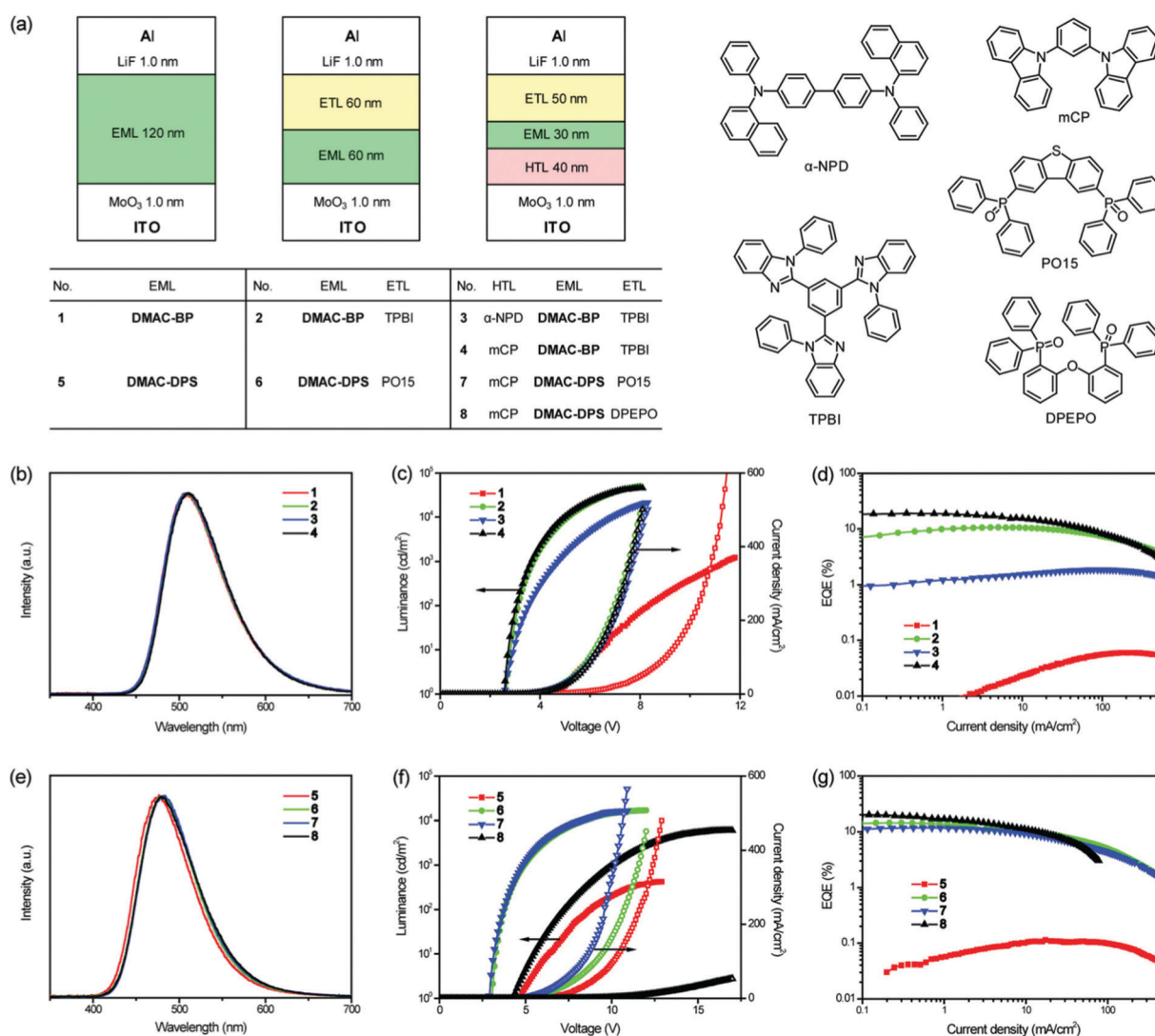
Fig. 12 (a) Structures of undoped OLEDs containing **DMAC-BP** or **DMAC-DPS** and the chemical structures of the hole-transport and electron-transport materials. (b) Electroluminescence spectra of **DMAC-BP**-based OLEDs at 1000 cd m^{-2}. (c) The luminance–current density–voltage characteristics of **DMAC-BP**-based OLEDs. (d) The EQE–current density characteristics of **DMAC-BP**-based OLEDs. (e) Electroluminescence spectra of **DMAC-DPS** based OLEDs at 1000 cd m^{-2}. (f) The luminance–current density–voltage characteristics of **DMAC-DPS** based OLEDs. (g) The EQE–current density characteristics of **DMAC-DPS** based OLEDs. Reproduced with permission from ref. 55. Copyright 2012 John Wiley & Sons.

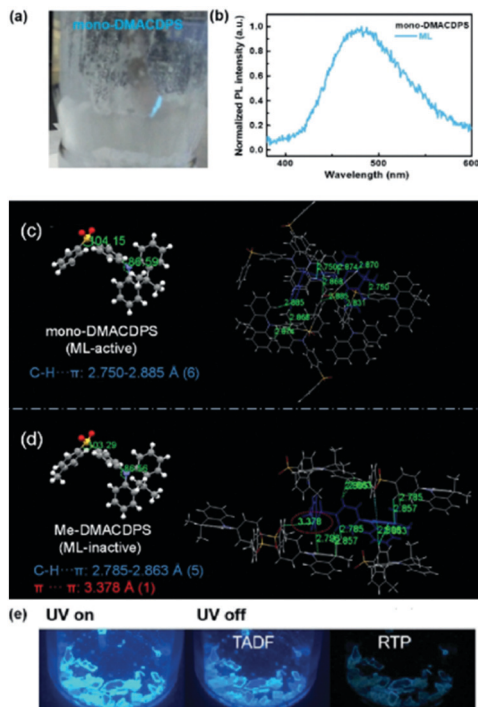Fig. 13 (a) The ML image of **DMAC-1DPS**. (b) ML spectrum in the crystal. (c and d) Crystal structures and intermolecular interactions for **DMAC-1DPS** and **Me-DMACDPS**, respectively. (e) Image of the **DMAC-1DPS** crystal with a 365 nm lamp on and off. Reproduced with permission from ref. 56. Copyright 2012 John Wiley & Sons.
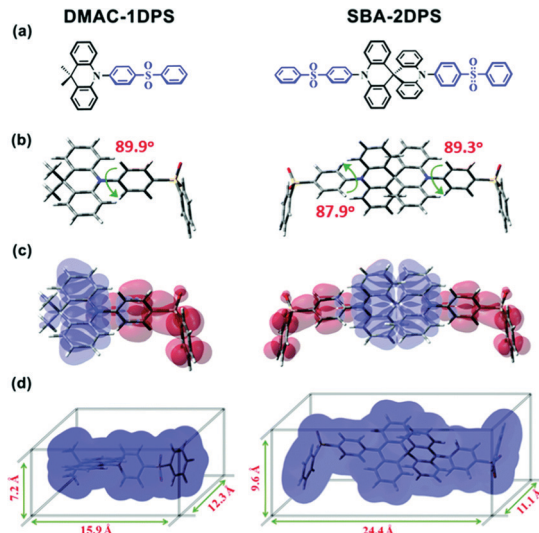

Fig. 14 (a) Molecular structures of **DMAC-1DPS** and **SBA-2DPS**. (b) Optimized ground state structures. (c) The HOMO (blue) and LUMO (red) distributions with optimized ground state structures. (d) Isodensity surface of the designed molecules with $r = 0.001$ e bohr^{-3}.

with a tight packing mode endowed **mono-DMACDPS** with strong ML (Fig. 13). The introduction of a methyl group reduced the number and intensity of molecular interactions. **Me-DMAC-DPS** exhibited strong π–π interactions, which was seriously detrimental to ML emission. The separated monomer and dimer in the crystal led to typical TADF and RTP properties, respectively. **mono-DMACDPS** was the first example realizing TADF, RTP, AIE, and ML simultaneously. In addition, it is worth noting that the ΔE_{ST} values of **DMAC-1DPS** and **Me-DMAC-DPS** were as low as 0.014 eV and 0.015 eV, respectively, indicating the possible existence of efficient RISC channels with high triplet exciton utilization.

Yang *et al.* further synthesized a TADF molecule, **SBA-2DPS** (Fig. 11), using **DPS** as the electron acceptor and spirodiacridine (**SBA**) as the electron donor.[51] The spiro-linked double D–A molecular architecture was introduced to selectively improve the horizontal emitting dipole orientation. Compared to the prototypical **DMAC-1DPS**, the shape of **SBA-2DPS** was elongated without expanding the degree of whole conjugation owing to the s-spacer linkage (Fig. 14). Consequently, a high horizontal dipole ratio of 87% was achieved for **SBA-2DPS**. The blue OLEDs based on **SBA-2DPS** showed a higher maximum EQE of 25.5% than **DMAC-1DPA**, with CIE coordinates of (0.15, 0.20). The effect of horizontal emission dipole and optical microcavity was considered to be an important factor to improve the EQE.

Subsequently, Su's team also constructed a similar TADF emitter **PX-SBA** (Fig. 11) by utilizing **SBA** as the central donor,

and **PX**, the two phenyl groups of **DPS** bridged by ether bonds, as the acceptor. Benefiting from the horizontal orientation and TADF feature, **PX-SBA** exhibited satisfactory electroluminescence performance overall. Pure blue emission with CIE coordinates of (0.16, 0.13) and an ideal EQE value of 20.8% were obtained in the doped devices.[57]

In 2019, Chi's group constructed two D–A–D* type TADF molecules, **4Cz-DPS** and **2Cz-DPS** (Fig. 11), by introducing a **Cz** donor unit at the *ortho*-position, in which the donor and acceptor groups were spatially in close proximity to guarantee the existence of intramolecular electrostatic attraction and through-space charge transfer.[58] Therefore two charge transfer pathways existed, namely bond charge transfer and space charge transfer (Fig. 15), which could enhance the radiation attenuation intensity of the emitter. The emission peak and photoluminescene quantum yield (PLQY) of pure films based on **4Cz-DPS** and **2Cz-DPS** were 530 nm and 74.7%, and 520 nm and 65.3%, respectively. In addition, **2Cz-DPS** also exhibited AIE properties, which were beneficial for the fabrication of non-doped devices. The non-doped devices based on **4Cz-DPS** and **2Cz-DPS** eventually achieved a maximum EQE of 20.7% and 28.7%, which represented one of the best performances of non-doped TADF-OLEDs.

Although **DPS** had been used widely as the an acceptor for blue TADF, the ΔE_{ST} of some molecules mentioned above was not small enough. Kido *et al.* proposed a solution in 2015, that is, to introduce another phenylsulfone into the **DPS** acceptor core to regulate the length of molecular π-conjugation and the electronic properties of the donor and acceptor, expecting to reduce ΔE_{ST}. TADF materials, **DTC-pBPSB** and **DTC-mBPSB** adopting (1,4-bis(benzenesulfonyl)benzene) and 1,3-bis(benzenesulfonyl) benzene as acceptors, were produced respectively.[59] It should be pointed out that **pBPSB**-based compounds possessed narrower energy band gaps and lower singlet and triplet energy

4504 | *J. Mater. Chem. C*, 2022, **10**, 4497–4520

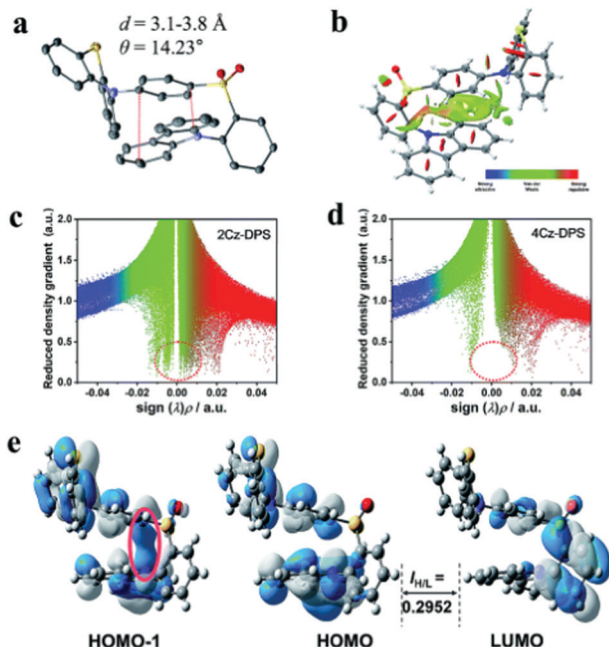This journal is © The Royal Society of Chemistry 2022

Fig. 15 (a) Single crystal and (b) reduced density gradient (RDG) isosurface map with an isovalue of 0.5 for **2Cz-DPS**. (c and d) The functions of RDG and Sign(λ_2)$_\rho$ for **2Cz-DPS** and **4Cz-DPS**, respectively. (e) HOMO and LUMO distribution of **2Cz-DPS**, showing the overlapping integral extents $I_{H/L}$.
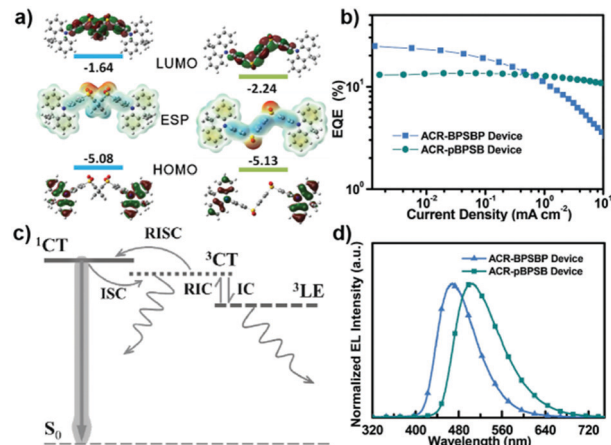

Fig. 16 (a) Calculated distributions and energy levels of the LUMO (top) and HOMO (bottom) and the molecular surface electrostatic potential (middle) in S_0 geometries (simulated at the B3LYP/6-31G* level, blue and red for positive and negative electrostatic potential, respectively). (b) EQE *versus* current density characteristics of the electroluminescence devices based on **ACR-BPSBP** and **ACR-pBPSB**. (c) The schematic diagram of influence came from the energy gap between two triplet states (^{3}CE and ^{3}LE) on the whole TADF process; S_0, ground state; IC, internal conversion; RIC, reverse internal conversion; ISC, intersystem crossing; RISC, reverse intersystem crossing. (d) EL spectra of the electroluminescence devices based on **ACR-BPSBP** and **ACR-pBPSB** measured at 5 mA cm^{-2}. Reproduced with permission from ref. 52. Copyright 2017 John Wiley & Sons.

levels compared with **mBPSB**-based isomers, due to the shorter effective conjugation and weaker electron-absorbing capacity. The ΔE_{ST} values of **DTC-pPBSB** and **DTC-mBPSB** were estimated to be 0.05 and 0.24 eV, respectively. **DTC-mBPSB**-based OLEDs exhibited deep blue CIE coordinates of (0.15, 0.08) with a maximum EQE of 5.5%, while **DTC-pBPSB** OLEDs exhibited sky blue CIE coordinates of (0.18, 0.19) with a maximum EQE of 11.7%. The small ΔE_{ST} and good device performance demonstrated the feasibility of the **BPSB** design and increased the variety of TADF acceptors based on phenylsulfone.

Kido and co-workers further put forward a strategy to achieve fluorescent materials simultaneously possessing a high-energy singlet CT state and triplet states, as well as an efficient radiative process *via* inserting a twisted core into the molecular backbone. In this work, the electron-donor **DTC** was replaced by 9,9-dimethyl-9,10-dihydroacridine (**ACR**) to generate **ACR-pBPSB**.

ACR-BPSBP (Fig. 11) was also prepared for studying the subtle influences of the inner-connection type on the molecular CT interactions.[52] According to DFT calculations (Fig. 16), the two benzene rings in the **BPSBP** core were almost orthogonal to each other, which made the two sulfonyl groups of **ACR-BPSBP** show a weak electron deficiency ability and led to an increased band gap, which eventually resulted in a shorter maximum emission wavelength. Besides, because of the high energy of the ^{3}CT state, the difference between E^0 (^{3}CT) and E^0 (^{3}LE) of **ACR-BPSBP** was relatively bigger than that of **ACR-pBPSB**, which suggested a relatively inefficient TADF process for **ACR-BPSBP**, and was proven by the following test of the lifetime of the

delayed fluorescence (τ_{DF}). For devices based on **ACR-pBPSB** and **ACR-BPSBP**, the maximum EL emission was observed at 468 nm and 502 nm, respectively. The CE of the device based on **ACR-pBPSB** was 37.6 cd A^{-1} and the maximum EQE was 13.5%. The CE of the device based on **ACR-BPSBP** was 38.7 cd A^{-1} and the EQE was 24.6%, which was almost doubled. The final results showed that the type of internal connection could influence the molecular CT interaction.

In fact, sulfone not only can be utilized to construct TADF emitters as the suitable acceptor, but also acts as a medium-strength acceptor for hot exciton materials. In 2015, Lu *et al.* reported a hot exciton material **PMSO** with a D–A–D structure by selecting **PPI** as a weak donor and **DPS** as a weak acceptor.[60] A highly mixed or hybrid local and charge transfer (HLCT) excited state would simultaneously achieve a large fraction of singlet formation and a high PLQY. The **PMSO**-based doped device displayed deep blue electroluminescence with emission peak at 445 nm and CIE coordinates of (0.152, 0.077). The maximum brightness, EQE, and CE were 15 599 cd m^{-2}, 6.80%, 4.64 cd A^{-1}, respectively. This work demonstrated the feasibility of HLCT molecular design in achieving efficient deep blue electroluminescence. Lu *et al.* reported deep-blue hybridized local and charge-transfer (HLCT) material compounds, **DP-TXO$_2$** and **P-TXO$_2$** (Fig. 17), in which 9,9-dimethylthioxanthene-S,S-dioxide (**TXO$_2$**) with a LUMO energy level of −2.33 eV was selected as the acceptor, and pyrene was used as the donor to ensure deep-blue emission.[61] To alleviate the intermolecular interactions between the pyrene subunit of the objective compounds and the 4,4',4''-tris(carbazol-9-yl)triphenylamine (TCTA, Fig. 20) host, a bulky 1,1':3,1''-terphenyl (TP) was grafted

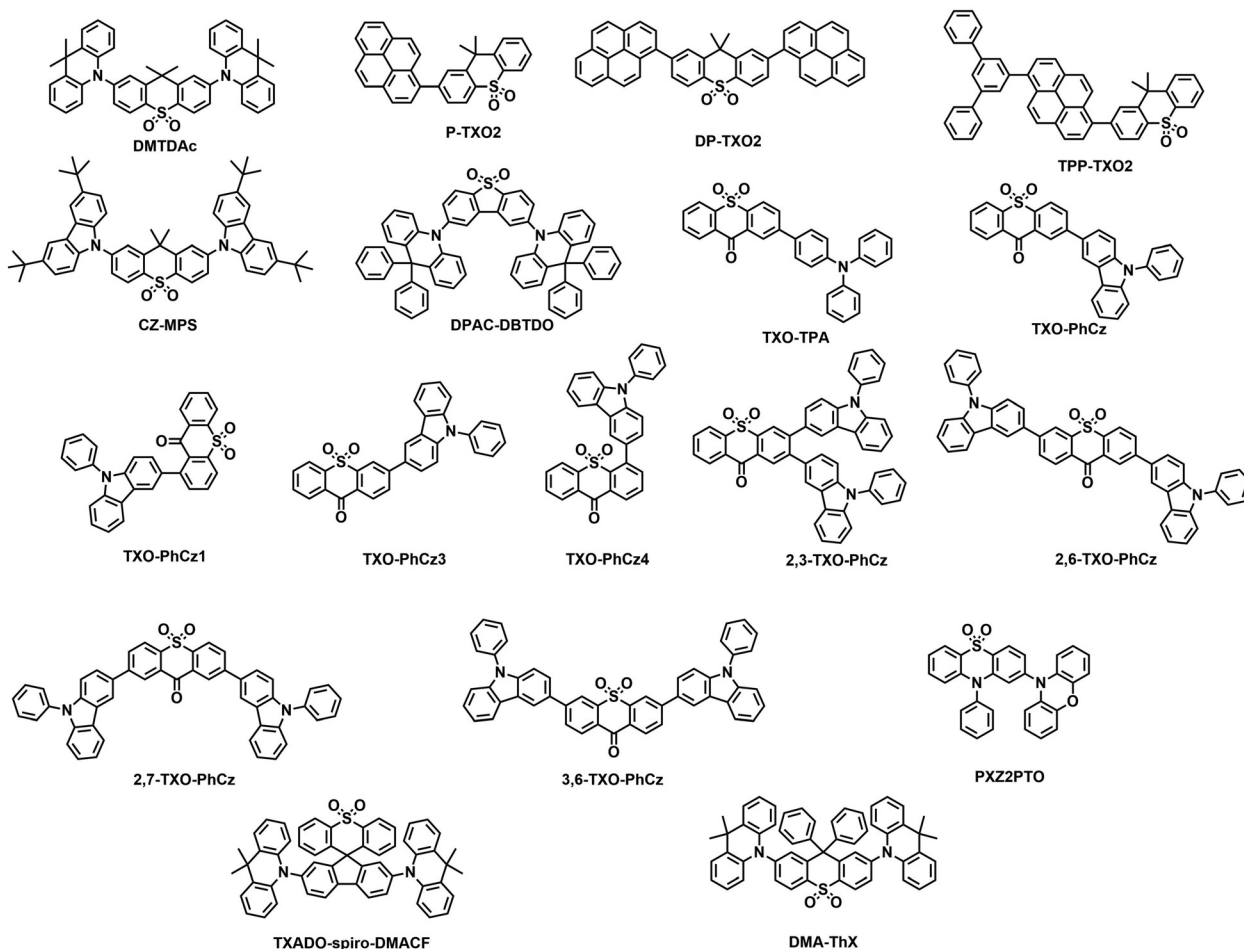This journal is © The Royal Society of Chemistry 2022

J. Mater. Chem. C, 2022, **10**, 4497–4520 | **4505**

Fig. 17 Molecular structures of the materials containing derivatives of **DPS**.

at the pyrene moiety of **P-TXO₂** to render **TPP-TXO₂**. As a result, **TPP-TXO₂** achieved the best device performance with CIE coordinates of (0.152, 0.065), EQE_{max} of 10.5%, as well as a high brightness of 10 480 cd m^{-2}. The maximum EUE of this device was even close to 100%.

Modification of the molecular structure of **DMAC-DPS** also could afford the TADF emitter in the deep blue region. Lee *et al.* reported the deep-blue light emitting molecule **DMTDAc** (Fig. 17) using a rigid 9,9-dimethyl-9*H*-thioxanthene-10,10-dioxide (**DMTD**) acceptor and an acridine donor, aiming to obtain high-efficiency deep blue TADF and a smaller FWHM than **DMAC-DPS**.[62] The inter-locking two phenyl units of **DPS** could reduce the molecular motion and shifted the emission color to the deep blue region. Therefore, the broad emission spectrum of the common TADF emitter became narrower by engineering the molecular structure to restrict the molecular motion. OLEDs based on **DMTDAc** achieved the CIE coordinates of (0.15, 0.13), a FWHM of 65 nm and an EQE close to 20%.

Subsequently, through interlocking of the **DPS** acceptor unit of a reported TADF emitter (**CZ-PS**)[53] by a dimethylmethylene bridge, **CZ-MPS** (Fig. 17), a UV-emissive TADF compound bearing a shallower LUMO energy level of −2.27 eV and a more rigid structure was achieved by Lu *et al.*[63] Compared with **DPS**, the two

phenyl groups of **MPS** were partially interlocked and bridged by dimethyl methyl. Moreover, the rigidity of **MPS** inhibited the intermolecular motion, which was conducive to the narrowing of the PL spectrum. The λ_{EL}, CIE coordinates, maximum brightness and EQE_{max} were obtained to be 389 nm, (0.175, 0.065), 1031 cd m^{-2} and 9.3%, respectively, for **CZ-MPS** doped OLED devices (Fig. 18). This work represented one of the highest efficiencies of UV-OLEDs.

Similar to **DMTD**, dibenzo[*B,D*]thiophene-5,5-dioxide (**DBTDO**) can also be utilized as a good acceptor with a rigid structure. In 2013, Monkman *et al.* carried out a detailed theoretical study on TADF molecules containing linear and angular **DBTDO** groups, and demonstrated that the material structure, that is, angular *versus* linear structures, and the presence of a ³nπ* triplet state and CT states with very small exchange energy were required to fully explain the observation of TADF in ICT materials with relatively large singlet ¹CT-triplet ³ππ* energy splitting.[64] This TADF mechanism was shown to be nearly 100% efficient in converting the triplet to singlet states. The key role of the ³nπ* could also explain the recent results of Adachi and co-workers who demonstrated near 100% internal quantum efficiency in a device where the ³CT state was higher in energy than the triplet energy of the host material used

4506 | *J. Mater. Chem. C*, 2022, **10**, 4497–4520

This journal is © The Royal Society of Chemistry 2022

Journal of Materials Chemistry C

Table 1 Summary of the device performances of emitters containing **DBT** units

Emitter	Emitting layer	$\lambda_{EL}{}^{a}$ [nm]	CE^{b} [cd A^{-1}]	PE^{c} [lm W^{-1}]	EQE^{d} [%]	CIE 1931 [x, y]	Ref.
DBT-BZ-DMAC	6 wt% emitter:CBP	508	51.7/31.1	50.7/17.2	17.9/10.9	0.234, 0.510	45
	emitter	516	43.3/43.1	35.7/33.1	14.2/14.2	0.261, 0.550	
DBT-BZ-PXZ	6 wt% emitter:CBP	528	60.6/48.6	59.2/21.8	19.2/15.4	0.340, 0.576	47
	emitter	557	26.6/19.6	27.9/11.3	9.2/6.8	0.434, 0.542	
DBT-BZ-PTZ	10 wt% emitter:CBP	538	46.0/29.5	43.3/13.6	15.1/9.7	0.370, 0.563	47
	emitter	563	26.5/23.5	29.1/15.4	9.7/8.5	0.448, 0.531	
DtBuAc-DBT	10 wt% emitter:DPEPO	455	13.9/-	9.7/-	10.5/-	0.133, 0.129	48

^{a} EL peak of the device. ^{b} The maximum value and value at 1000 cd m^{-2} of current efficiency. ^{c} The maximum value and value at 1000 cd m^{-2} of power efficiency. ^{d} The maximum value and value at 1000 cd m^{-2} of EQE.

Table 2 Summary of the device performances of emitters containing **DPS** units

Emitter	Emitting layer	$\lambda_{EL}{}^{a}$ [nm]	CE^{b} [cd A^{-1}]	PE^{c} [lm W^{-1}]	EQE^{d} [%]	CIE 1931 [x, y]	Ref.
DPA-DPS	10 wt% emitter:DPEPO	421	—	—	2.9	—	53
TDPA-DPS	10 wt% emitter:DPEPO	430	—	—	5.6	—	
TDTC-DPS	10 wt% emitter:DPEPO	423	—	—	9.9	0.15, 0.07	
DMOC-DPS	10 wt% emitter:DPEPO	460	24.0/—	—	14.5/3.7	0.16, 0.16	54
PXZ-DPS	Emitter:CBP	—	—	—	17.5/15.5	—	50
DMAC-DPS	Emitter:DPEPO	470	—	—	19.5/16.0	0.16, 0.20	55
	Emitter	480	—	—	19.5/14.6	0.16,0.29	
DMAC-1DPS	30 wt% emitter:DPEPO	477	31.0/20.9	30.5/10.9	17.4/11.6	0.16,0.26	56
SBA-DPS	30 wt% emitter:DPEPO	467	38.1/23.5	37.4/12.3	25.5/15.6	0.15, 0.20	51
PX-SBA	20 wt% emitter:DPEPO	448	24.4/8.3	24.0/3.7	20.8/7.0	0.16, 0.15	57
4Cz-DPS	Emitter	524	61.2/—	38.4/—	20.7/—	—	58
2Cz-DPS	Emitter	518	82.3/—	51.8/—	28.7/—	—	
DTC-mBPSB	10 wt% emitter:DPEPO	≈444	4.4/—	—	5.5/—	0.15, 0.08	59
DTC-pBPSB	10 wt% emitter:DPEPO	≈474	19.4/—	—	11.7/—	0.18, 0.19	
ACR-pBPSB	20 wt% emitter:mCP	502	37.6/—	—	13.5/—	0.16, 0.21	52
ACR-BPSBP	20 wt% emitter:DPEPO	468	38.7/—	—	24.6/—	0.27, 0.48	
PMSO	10 wt% emitter:CBP	445	4.64/—	4.00/—	6.80/5.64	0.152, 0.07	60
	Emitter	465	7.31/—	6.23/—	4.95/4.86	0.157, 0.206	
DMTDAc	30 wt% emitter:UGH3/TSPO1	451	22.6/—	23.2/—	19.8/—	0.15, 0.13	62
P-TXO2	12 wt% emitter:TCTA/12 wt% emitter:26DCzPPy	452	3.0/—	—	4.0/3.4	0.106, 0.085	61
DP-TXO2	12 wt% emitter:TCTA/12 wt% emitter:26DczPPy	462	4.6/—	—	4.0/3.5	0.154, 0.098	
TPP-TXO2	12 wt% emitter:TCTA/12 wt% emitter:26DczPPy	443	11.1/—	—	10.5/4.6	0.152, 0.065	
CZ-MPS	10 wt% emitter:TCTA/10 wt% emitter:CzSi	389	3.4/—	—	9.3/	0.175, 0.065	63
DPAC-DBTDO	15 wt% emitter:DPEPO	500	34.2/—	26.3/—	13.1/5.7	0.252, 0.455	65
TXO-TPA	5 ± 1 wt% emitter:mCP	552	43.3/—	47.7/—	18.5/—	0.45, 0.53	66
TXO-PhCz	5 ± 1 wt% emitter:mCP	—	76.0/—	70.0/—	21.5/—	0.31, 0.56	
TXO-PhCz3	10 wt% emitter:mCP	532	45.3/6.8	35.6/2.2	14.0/2.1	0.40, 0.54	68
TXO-PhCz4	6 wt% emitter:PPO21	540	49.4/26.8	47.714.7	16.3/9.0	0.38, 0.55	
2,3-TXO-PhCz	15 wt% emitter:CBP	—	37.2/—	27.8/—	11.9/—	0.42, 0.55	69
2,6-TXO-PhCz	8 wt% emitter:CBP	—	72.3/—	64.9/—	23.2/—	0.40, 0.55	
2,7-TXO-PhCz	15 wt% emitter:CBP	—	74.6/—	68.9/—	24.4/—	0.39, 0.55	
3,6-TXO-PhCz	8 wt% emitter:CBP	—	54.3/—	48.8/—	18.1/—	0.43, 0.53	
PXZ2PTO	Emitter	504	44.9/—	32.0/—	16.4/—	0.27, 0.50	70
TXADO-spiro-DMACF	Emitter	444	5.3/—	5.9/—	5.3/—	0.16, 0.09	71
DMA-ThX	Emitter:DPEPO	462	18.2/—	—	18.4/—	0.14, 0.14	72

^{a} EL peak of the device. ^{b} The maximum value and value at 1000 cd m^{-2} of current efficiency. ^{c} The maximum value and value at 1000 cd m^{-2} of power efficiency. ^{d} The maximum value and value at 1000 cd m^{-2} of EQE.

which should efficiently quench the ^{3}CT state. Both the ^{3}n$\pi^{\star}$ and $^{3}\pi\pi^{\star}$ states would be lower in energy than the host so as to avoid quenching. In 2016, Lu *et al.* prepared a TADF molecule **DPAC-DBTDO** (Fig. 17) with a D–A–D structure by using **DBTDO** as the acceptor and 9,9-diphenyl-9,10-dihydroacridine (**DPAC**), which possessed large steric hindrance and a rather high triplet energy when substituted on the 9-site, as the donor.[65] The PL and transient fluorescence spectra showed that **DPAC-DBTDO** possessed a small ΔE_{ST} of 0.10 eV, which was favorable for an efficient RISC process. The doped OLEDs exhibited stable blue-green fluorescence with the CIE coordinates of (0.252, 0.455), a maximum CE of 34.2 cd A^{-1}, and an EQE_{max} of 13.1%.

In addition to **DMTD** and **DBTDO**, TADF based on other rigid phenyl sulfones also attracted much attention. In 2014, Wang's group synthesized two novel **TX**-based emitters with excellent TADF properties, **TXO-TPA** and **TXO-PhCz** (Fig. 17). Both of them had a typical D–A structure with 9-*H*-thioxanthen-9-one-10,10-dioxide (**TXO**) as the acceptor and triphenyl-amine (**TPA**)/N-phenylcarbazole (**N-PhCz**) as the donor.[66] The AIE characters of **TXO-PhCZ** and **TXO-TPA** were observed in

Table 3 Summary of the device performances of emitters containing **BZ** units

Emitter	Emitting layer	$\lambda_{EL}{}^a$ [nm]	CE^b [cd A^{-1}]	PE^c [lm W^{-1}]	EQE^d [%]	CIE 1931 [x, y]	Ref.
TPA-BZP	Emitter	588	8.84/7.92	7.18/4.64	3.80/3.41	0.55, 0.45	74
CzP-BZP	Emitter	538	23.99/13.18	16.38/8.82	6.95/3.81	0.34, 0.60	75
BTH-DMF	30 wt% emitter:SPPO1	550	31.02/16.95	27.85/8.43	9.13/4.94	0.41, 0.56	76
2F-BTH-DMF	30 wt% emitter:SPPO1	515	26.62/12.57	26.14/5.25	8.52/4.02	0.29, 0.54	
o-BTH-DMF	30 wt% emitter:SPPO1	454	1.73/0.79	1.16/0.40	1.51/0.69	0.15, 0.13	
PTZ-BZP	Emitter	692	—	—	1.54/—	0.69, 0.30	36
BTDF-TTPA	Emitter	690	0.11/—	0.09/—	0.83/—	0.70, 0.30	77
	1 wt% emitter:CBP	630	5.15/—	4.27/—	5.75/—	0.61, 0.34	
BTDF-TtTPA	Emitter	690	0.19/—	0.16/—	1.44/—	0.71, 0.29	
	1 wt% emitter:CBP	642	2.98/—	2.60/—	4.94/—	0.63, 0.33	
TPABTPA	Emitter	608	17.7/—	12.4/—	11.1/—	0.59, 0.40	78
	Emitter:CBP	608			18.1	0.58, 0.41	
TPABCHO	Emitter	640	4.7/—	2.5/—	5.0/—	0.64, 0.36	
	Emitter:CBP	590			8.9	0.54, 0.45	

^{a} EL peak of the device. ^{b} The maximum value and value at 1000 cd m^{-2} of current efficiency. ^{c} The maximum value and value at 1000 cd m^{-2} of power efficiency. ^{d} The maximum value and value at 1000 cd m^{-2} of EQE.

Table 4 Summary of the device performances of emitters containing **NZ** units

Emitter	Emitting layer	$\lambda_{EL}{}^a$ [nm]	CE^b [cd A^{-1}]	PE^c [lm W^{-1}]	EQE^d [%]	CIE 1931 [x, y]	Ref.
TPA-NZP	Emitter	664	1.00/—	0.77/—	2.8/—	0.67, 0.32	79
TPA-NZC	Emitter	702	—	—	1.2/—	0.685, 0.299	80
	6 wt% emitter:CBP	656	—	—	3.2/—	0.657, 0.335	
NZ2TPA	Emitter	696	—	—	3.9/2.8	0.70, 0.30	81
NZ2AC	Emitter	663	2.6/—	2.0/—	2.8/2.0	—	82
	8 wt% emitter:CBP	612	11.2/—	11.3/—	6.2/2.4	—	
PXZ-3-NZP	Emitter	738	—	—	0.82/—	0.703, 0.289	83
	7wt% emitter:MADN	672	—	—	2.03/—	0.686, 0.306	
PXZ-10-NZP	Emitter	680	—	—	0.077/—	0.687, 0.304	
	7wt% emitter:MADN	640	—	—	0.60/—	0.644, 0.354	
TNZPPI	Emitter	686	0.40/—	0.47/—	2.48/—	0.69, 0.30	73
	10 wt% emitter:CBP	648	3.45/—	2.63/—	6.83/—	0.67, 0.33	
TNZtPPI	Emitter	686	0.30/—	0.33/—	1.60/—	0.69, 0.31	
	5 wt% emitter:CBP	642	4.01/—	3.31/—	6.52/—	0.64, 0.35	
TNZ2tPPI	Emitter	678	0.31/—	0.32/—	1.48/—	0.69, 0.31	
	10 wt% emitter:CBP	654	1.94/—	1.59/—	4.83/—	0.67, 0.33	

^{a} EL peak of the device. ^{b} The maximum value and value at 1000 cd m^{-2} of current efficiency. ^{c} The maximum value and value at 1000 cd m^{-2} of power efficiency. ^{d} The maximum value and value at 1000 cd m^{-2} of EQE.

Table 5 Summary of the device performances of emitters containing **PTZ** units

Emitter	Emitting layer	$\lambda_{EL}{}^a$ [nm]	CE^b [cd A^{-1}]	PE^c [lm W^{-1}]	EQE^d [%]	CIE 1931 [x, y]	Ref.
PTZ-TRZ	2 wt% emitter:mCBP	532	—	—	10.8 ± 0.5/—	—	86
PTZ-DBPHZ	10 wt% emitter:CBP	613	19.6/—	—	16.8/—	—	93
CP-BP-PTZ	Emitter	554	46.1/38.4	55.7/30.2	15.3/12.7	0.42, 0.55	95
	10 wt% emitter:CBP	542	62.4/43.4	57.3/22.0	19.6/13.6	0.38, 0.57	
PTZ-TTR	14.7 wt% emitter:CBP	448, 584	5.20/1.75	4.93/0.82	2.68/0.93	0.33, 0.33	98
PTZ-Ph-TTR	1.2 wt% emitter:CBP	456, 568	45.21/30.55	41.75/19.58	16.34/11.04	0.41, 0.47	
PTZ-BP	4 wt% emitter:DCzDPy	440, 540	16.6/—	13.0/—	6.2/—	0.34, 0.46	100
	4 wt% emitter:CBP	—	15.5/—	—	5.44/—	—	
PTZ-Mes$_2$B	Emitter	540	62.88/—	—	19.66/17.31	0.37, 0.57	101
PTZ-ND	7.5 wt% emitter:mCP	528	40.9/34.3	31.4/22.0	13.0/11.0	0.30, 0.50	102
pipd-BZ-PTZ	6 wt% emitter:CBP	545	55.41/40.92	58.03/27.95	15.77/12.40	0.31, 0.57	103
	20 wt% emitter:CBP	550	38.70/37.80	31.05/26.99	12.03/11.76	0.42, 0.55	

^{a} EL peak of the device. ^{b} The maximum value and value at 1000 cd m^{-2} of current efficiency. ^{c} The maximum value and value at 1000 cd m^{-2} of power efficiency. ^{d} The maximum value and value at 1000 cd m^{-2} of EQE.

water/acetonitrile mixtures, with PLQYs of 0.93 ± 0.02 and 0.36 ± 0.02 for films, respectively. The ΔE_{ST} were estimated to be 0.04 eV for **TXO-TPA** and 0.09 eV for **TXO-PhCz**. The maximum EQE value of **TXO-TPA** and **TXO-PhCz** reached 21.5% and 18.5%, respectively (Fig. 19). It was the record level for OLEDs based on the TADF mechanism at that time.
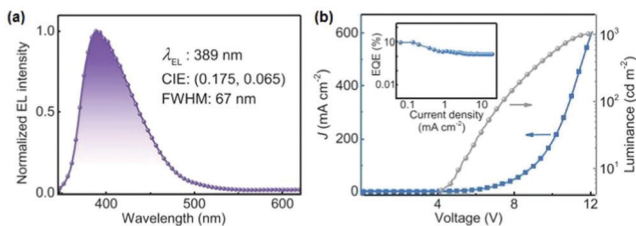
4508 | *J. Mater. Chem. C*, 2022, **10**, 4497–4520

This journal is © The Royal Society of Chemistry 2022

Fig. 18 (a) EL spectrum of the **CZ-MPS**-based OLEDs at a current density of 100 mA cm^{-2}. (b) Current density–voltage–luminance (J–V–L) characteristics of the **CZ-MPS**-based OLEDs. Inset: EQE–current density curve of the **CZ-MPS**-based OLEDs. Reproduced with permission from ref. 63. Copyright 2020 John Wiley & Sons.
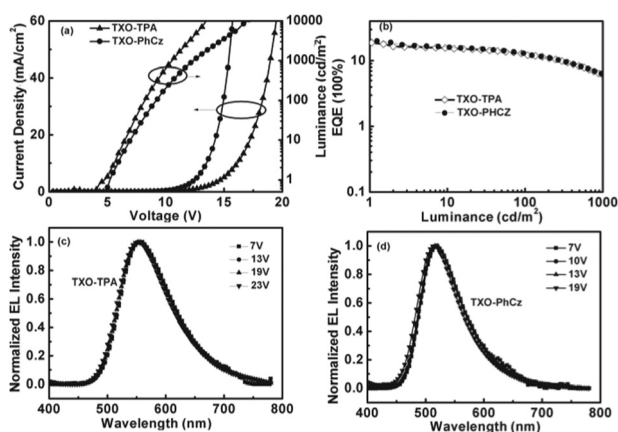

Fig. 19 (a) Current density–voltage–luminance characteristics of the OLEDs based on compounds **TXO-TPA** and **TXO-PhCz**. (b) The EQE–current density characteristics. (c) The EL spectra when operated at different voltages of the device incorporating **TXO-TPA**. (d) The EL spectra when operated at different voltages of the device incorporating **TXO-PhCz**. Reproduced with permission from ref. 66. Copyright 2014 John Wiley & Sons.

And then, in 2016, they further optimized the host material of the OLEDs and selected 1,3,5-tris(N-phenylbenzimidazole-2-yl)benzene (TPBI) as the doped host to adjust the interaction between the host and guest.[67] Strong interaction between **TXO-PhCz** and TPBI could be observed, leading to the lower singlet–triplet energy gap of 8.8 meV and non-monotonic increase of PLQYs (Φ_{Totle}, Φ_{D}, and Φ_{P}) with temperature. Finally, the performance of the **TXO-PhCz**-based device was further improved, achieving a maximum CE of 71.9 cd A^{-1}, a maximum power efficiency of 45.2 lm W^{-1} and a maximum EQE of 23.2%. This work demonstrated the importance of choosing the right host for the EL performance.

In 2017, they further designed three D–A isomers based on **TXO, TXO-PhCz1, TXO-PhCz3** and **TXO-PhCz4** (Fig. 17) to study the effect of **PhCz** substituted at different positions.[68] **TXO-PHCz4** exhibited strong orbital coupling resulting in strong phosphorescence emission, which eventually caused the inverse temperature dependence of the transient PL decay, contrary to that of **TXO-PhCz3** and other TADF emitters. **TXO-PhCz4** exhibited a small ΔE_{ST} of 23 meV and a short decay time of 14 ms at room temperature, which were much smaller and

shorter than those of **TXO-PhCz3** and made the efficiency roll-off of the device very slight. The maximum CE, PE and EQE of the devices containing **TXO-PhCz4** were 45.6 cd A^{-1}, 35.8 lm W^{-1} and 15.4%, respectively.

In 2018, they further reported four D–A–D isomers, **2,3-TXO-PhCz, 2,6-TXO-PhCz, 2,7-TXO-PhCz**, and **3,6-TXO-PhCz** (Fig. 17).[69] The substitution positions of the two **PhCz** units significantly impacted the photophysical properties of the isomers, especially for the ΔE_{ST} and oscillator strength (f) (Fig. 21). The four emitters possessed a small ΔE_{ST} of 0.01–0.24 eV; the corresponding f values were 0.064, 0.107, 0.026, and 0.134. This result indicated that 3-position substitution contributed to the increase of f and thus improved the PLQY. The device based on **2,7-TXO-PhCz** achieved the best device performance: 74.6 cd A^{-1} for CE, 68.9 lm W^{-1} for PE, and 24.4% for EQE. This work showed that the ΔE_{ST} and f played a synergistic role in OLED performance.

TADF materials that can exhibit high efficiency in non-doped OLEDs are of significant importance. In 2018, Wang et al. reported an emitter **PXZ2PTO** (Fig. 17) which contained phenoxazine as the donor and **2PTO** as the acceptor, exhibiting both AIE characteristics and TADF properties.[70] **PXZ2PTO** exhibited a small ΔE_{ST} of 0.02 eV and a high PLQY of 68.75% in doped films and 61.54% in pure films. **PXZ2PTO** showed high efficiency in both undoped and doped devices. Green TADF non-doped OLEDs achieved a maximum EQE, CE and PE of 16.4%, 44.9 cd A^{-1} and 32.0 lm W^{-1}, respectively, which was comparable to those of the doped OLEDs. These results indicated that **PTZ**-oxide could be a good acceptor for the design of aggregation induced delayed fluorescence (AIDF) materials.

Spiro-blocking is also a promising strategy to develop deep-blue TADF emitters capable of application in non-doped OLEDs. In 2019, Ding et al. reported a deep-blue TADF emitter **TXADO-spiro-DMACF** (Fig. 17) by integrating an appropriate blocking unit with the D–A–D-type TADF emitter via a spiro linkage.[71] The intermolecular interactions were weakened to some degree benefiting from the characteristic perpendicular arrangement. As a result, **TXADO-spiro-DMACF** showed a very small bathochromic shift of 8 nm associated with a narrowed FWHM of 54 nm from solution to film. The corresponding non-doped device successfully achieved a bright deep-blue emission, revealing CIE coordinates of (0.16, 0.09) and a peak EQE of 5.3% (5.3 cd A^{-1}, 5.9 lm W^{-1}).

In 2019, Kim et al. synthesized a TADF material **DMA-ThX** (Fig. 17) using a simple process.[72] **DMA-ThX** showed twisted moieties, and the bandgap was found to be sufficiently large to radiate deep-blue light with high-lying HOMO and LUMO energy levels of −5.77 and −2.37 eV, respectively. A small ΔE_{ST} of 0.07 eV for the TADF emission process was demonstrated by the extremely fast PL lifetimes of the **DMA-ThX** solution and films at room temperature and low temperature, which was in the order of 10^{-8} s. OLEDs reached a maximum EQE of 18.4% with CIE coordinates of (0.14, 0.14) when **DMA-ThX** was doped with bis[2-(diphenylphosphino) phenyl]ether oxide (DPEPO, Fig. 20), and the FWHM of the device was 65 nm.
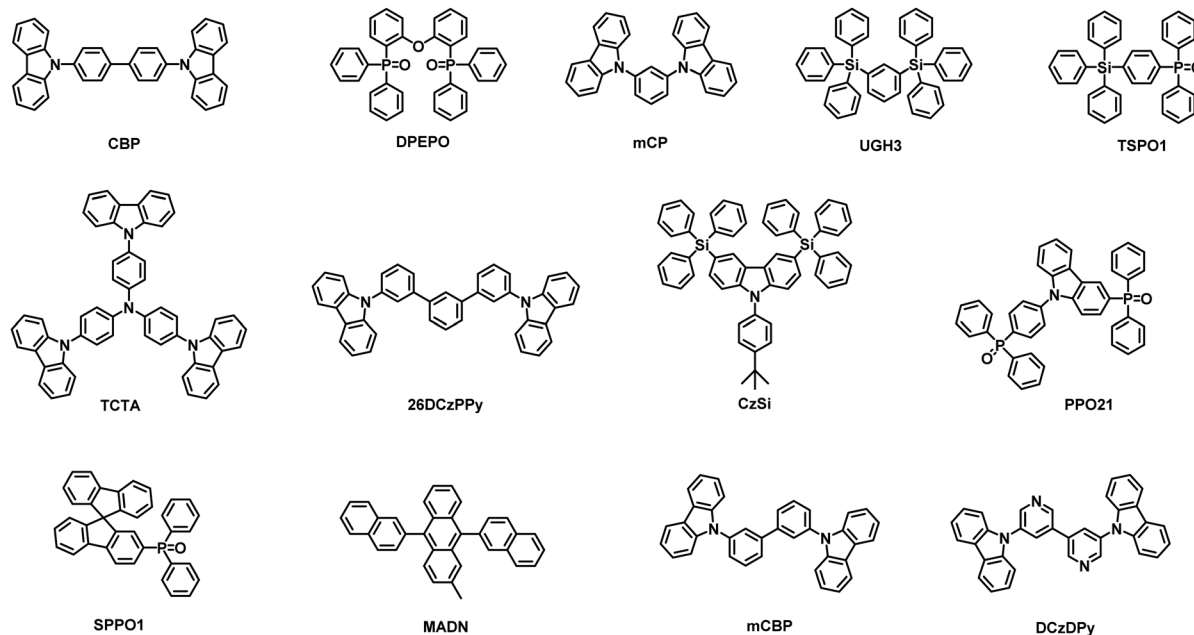
CBP **DPEPO** **mCP** **UGH3** **TSPO1**

TCTA **26DCzPPy** **CzSi** **PPO21**

SPPO1 **MADN** **mCBP** **DCzDPy**

Fig. 20 Molecular structures of the materials used as the host in the emitting layers of the devices listed in Tables 1–5.
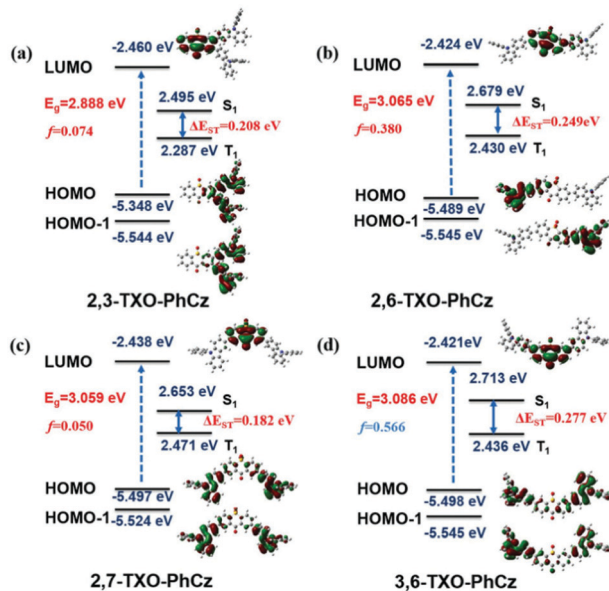

Fig. 21 (a–d) HOMO, HOMO−1, and LUMO electronic distributions, energy level, and bandgaps (E_g), the lowest singlet (S_1), and triplet (T_1) and oscillator strengths of S_1 (f) for **2,3-TXO-PhCz**, **2,6-TXO-PhCz**, **2,7-TXO-PhCz**, and **3,6-TXO-PhCz** calculated using the TD-DFT at the B3LYP/6-31G** level, respectively. Reproduced with permission from ref. 69. Copyright 2018 John Wiley & Sons.

2.3 BZ/NZ based emitters

As two main derivatives of thiazoles used in OLED emitters, **BZ** and **NZ** have been widely used in the construction of hot exciton materials.[36,73] The energy gap between the T_1 and T_2 states of **BZ** is large, and at the same time the energy gap between the S_1 and T_2 states is small, which meets the design concept of hot exciton materials.

In 2014, Ma and his colleagues reported a **BZ**-based molecule, **TPA-BZP** (Fig. 22), and further elaborated the emission mechanism of hot exciton materials through detailed characterization of **TPA-BZP** and its related molecules.[74] The non-doped OLED device of **TPA-BZP** achieved a maximum EQE of 3.8%. The maximum exciton utilization efficiency (EUE) was harvested up to 93%. Through the energy-level structure of the excited states, the hot exciton mode was proposed to be responsible for these large breakthroughs in exciton utilization efficiency.

In 2016, Ma *et al.* further developed another molecule **CzP-BZP** (Fig. 22) on the basis of former **TPA-BZP**.[75] By switching the donor unit, that is, the stronger donor **TPA** was replaced by the weaker donor carbazobenzene (**CzP**), the relative distribution ratio of the LE state and CT state in **CzP-BZP** greatly changed (Fig. 23), and the PLQY of films based on **CzP-BZP** was increased by 30%. The EUE of 48% in **CzP-BZP** was also comparable to that of 42% in **TPA-BZP**. **CzP-BZP** exhibited an excellent EL performance in non-doped devices, achieving a maximum EQE of 6.95% and a maximum CE of 23.99 cd A^{-1} with a CIE of (0.34, 0.60).

In 2018, Wang *et al.* designed and synthesized three D–A–D molecules **2F-BTH-DMF**, **BTH-DMF**, and **o-BTH-DMF** (Fig. 22) applying **BZ** as the acceptor.[76] The 4,7-bis(9,9-dimethyl-9*H*-fluoren-2-yl) (**DMF**) unit was introduced due to its rigid and planar structure with weak electron-donating properties. The RISC process *via* the high-lying triplet state, also called the hot exciton mechanism, was adequately demonstrated by the steady and transient photophysical results combined with DFT calculations (Fig. 24). The PLQY of **BTH-DMF** and **2F-BTH-DMF** was as high as 90.4% and 97.7%, respectively. The three emitters all showed high RISC rate constants k, and the k_{RISC} of **BTH-DMF** and **2F-BTH-DMF** reached 10^6 s^{-1}, which were higher than the 10^5 s^{-1} of **o-BTH-DMF**, making the oxygen

4510 | *J. Mater. Chem. C*, 2022, **10**, 4497–4520

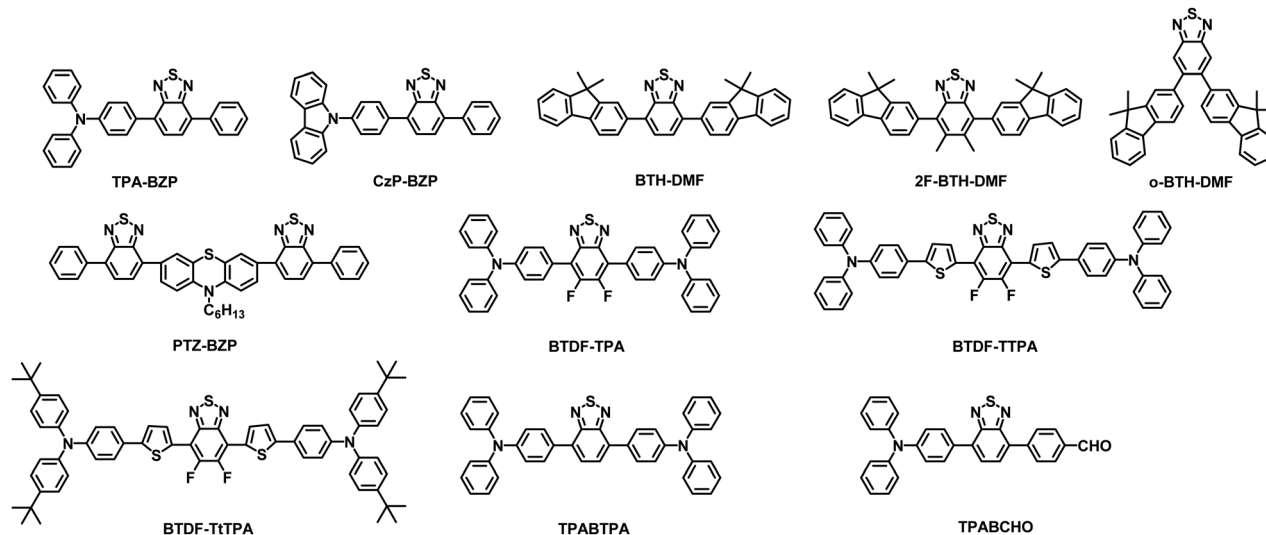This journal is © The Royal Society of Chemistry 2022

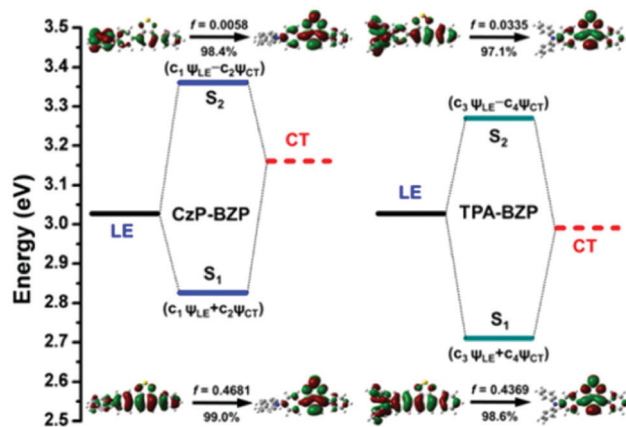Fig. 22 Molecular structures of the materials containing **BZ** units.

Fig. 23 Hybridization between LE and CT states at the geometry of the S_1 state of **CzP-BZP** and **TPA-BZP**, respectively. Reproduced with permission from ref. 75. Copyright 2016 American Chemical Society.

quenching of **o-BTH-DMF** more obvious. The **BTH-DMF** device exhibited impressive CE, PE, and EQE up to 31.02 cd A^{-1}, 27.85 lm W^{-1}, and 9.13% with a maximum brightness of 25 400 cd m^{-2}, respectively.

As mentioned above, weak donor bonding with **BZ** could produce yellow-green fluorescence. Therefore, for these D–A structure molecules, a stronger donor unit could red-shift the butterfly phenothiazine **PTZ** donor.[36] The maximum emission peak was at 700 nm with a PLQY of 16% in thin films. The maximum EQE of undoped NIR OLEDs based on **PTZ-BZP** reached 1.54% and a low efficiency roll-off was observed, as well as a high radiative exciton ratio of 48%, which broke through the limit of 25% in conventional fluorescent OLEDs. According to DFT calculations, there existed a large energy level difference between the T energy levels, and the ΔE_{ST} of the S_1 and T_3 states was close to 0 (Fig. 25), which provided an efficient RISC channel. This work provided a new idea for the design of efficient NIR fluorescent molecules.

In 2019, Su *et al.* synthesized three orange-yellow to NIR hot exciton emitters, **BTDF-TPA**, **BTDF-TTPA**, and **BTDF-TtTPA** (Fig. 22).[77] By introducing thiophene as a π bridge into the D–A–D framework, the conjugation length of **BTDF-TTPA** and **BTDF-TtTPA** was extended, and the dihedral angle between the donor and acceptor was reduced, which led to a high FMO overlap. Therefore, the emission peak positions of the two compounds were red shifted 67 nm relative to **BTDF-TPA** without changing the PLQY. The maximum EQEs of **BTDF-TTPA** and **BTDF-TtTPA** were 5.75% and 4.94%, respectively. The non-doped device based on the latter achieved a maximum EQE of 1.44% peaking at 690 nm in NIR emission.

In 2019, Chi *et al.* reported two red emitters, **TPABTPA** and **TPABCHO**, based on the hot exciton mechanism.[78] According to theoretical calculations, the triplet excitons of **TPABTPA** and **TPABCHO** attenuated mainly through $T_2/T_3 \rightarrow S_1$. **TPABTPA** and **TPABCHO** enabled non-doped OLEDs with excellent EQEs of 11.1% and 5.0% (Fig. 26), attributing to the high EUE of 82% and 46%, respectively. Such a high non-doped EQE was rarely observed in red OLEDs. They could also be utilized in white OLEDs. After appropriate device structure design, pure fluorescent WOLEDs were obtained with a maximum EQE of 23.0% and relatively stable white light emission CIE coordinates of (0.34, 0.33). As one of the best results, the **NZ** unit also possessed a large T_2–T_1 energy gap and pure fluorescent WOLEDs, and it provided a method to achieve HLCT-TADF pure fluorescent WOLEDs with high performance and similar orbital symmetry between T_1 and T_2, which can effectively inhibit IC from T_2 to T_1. Thus, it is the most widely used building block for deep-red and NIR hot exciton materials. In 2013, Ma's team reported a deep red emitter, **TPA-NZP** (Fig. 27), with intercrossed LE and CT characters, demonstrated by the solvatochromic experiment and density functional theory (DFT) calculations.[79] The PL properties and lifetime measurements of **TPA-NZP** in different solvents showed that the excited state of **TPA-NZP** in medium polar solvents was a HLCT state.
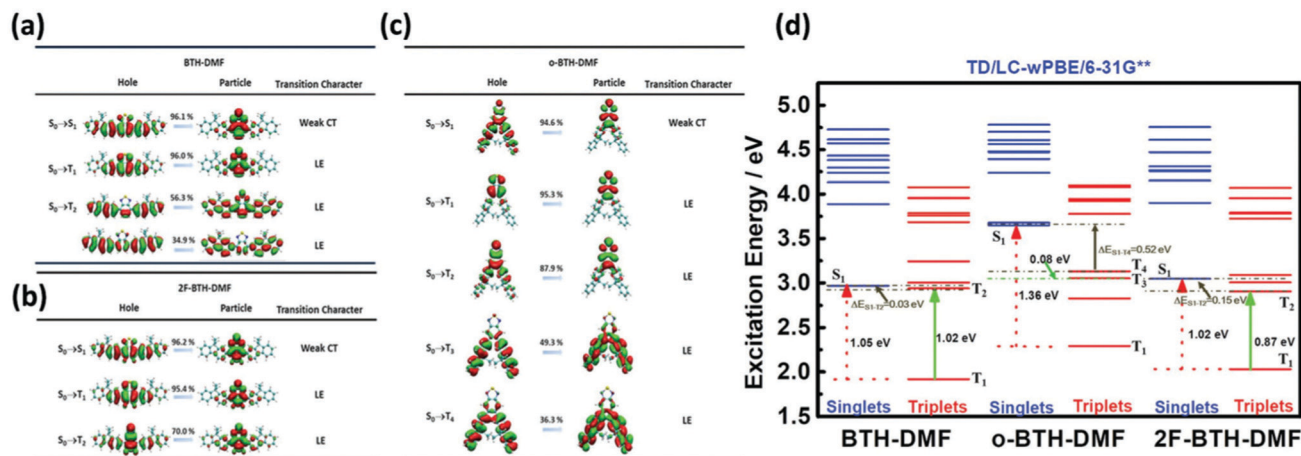
This journal is © The Royal Society of Chemistry 2022

J. Mater. Chem. C, 2022, **10**, 4497–4520 | **4511**

Fig. 24 Theoretical calculation for the three compounds: natural transition orbital (NTO) pairs for the excited states of **BTH-DMF** (a), **2F-BTH-DMF** (b), and **o-BTH-DMF** (c), respectively. (d) The energy diagram of the first ten singlet and triplet excited states of **BTH-DMF**, **2F-BTH-DMF**, and **o-BTH-DMF**. Reproduced with permission from ref. 76. Copyright 2018 John Wiley & Sons.
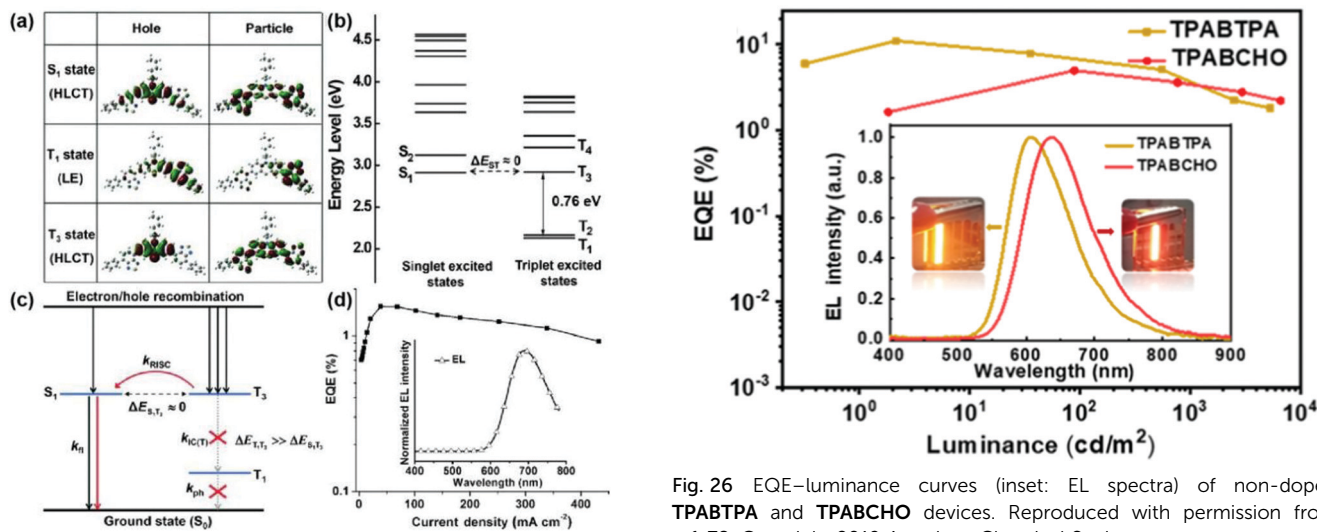

Fig. 25 (a) Natural transition orbitals for S_1, T_1, and T_3 states of **PTZ-BZP**. (b) The energy landscape for singlet and triplet excited states. (c) Model for exciton relaxation in the EL process. RISC: reverse intersystem crossing; IC(T): internal conversion between the triplet states; fl: fluorescence; ph: phosphorescence. (d) EQE–current–density characteristics of the device. The inset graph shows the EL spectrum. Reproduced with permission from ref. 36. Copyright 2014 John Wiley & Sons.

Fig. 26 EQE–luminance curves (inset: EL spectra) of non-doped **TPABTPA** and **TPABCHO** devices. Reproduced with permission from ref. 78. Copyright 2019 American Chemical Society.

Using **TPA-NZP** as the active layer in OLEDs, high EUE values of 93% (at low brightness) and 50% (at excitons) were achieved in the OLEDs. The emission peak of non-doped OLEDs was at 664 nm with a CIE of (0.67, 0.32), and the maximum EQE reached 2.8%. This work provided an important design idea for future HLCT materials with red or even deeper colors.

Yang and colleagues subsequently reported the hot exciton material **TPA-NZC** (Fig. 27).[80] Compared with **TPA-NZP**, **TPA-NZC** contained an additional cyanide group as a co-acceptor, which enhanced the acceptor capacity of **NZ** in D–A molecules. Compared with **TPA-NZP** (668 nm and PLQY of 15%), **TPA-NZC**
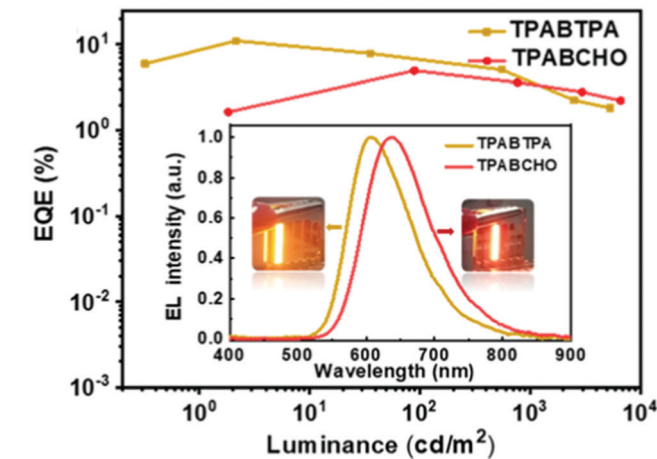
exhibited an NIR emission of 710 nm with a large red-shift, as well as a maintained PLQY of 17% in films. Quantum chemical calculations and photophysical characterization showed that **TPA-NZC** exhibited HLCT characteristics, which contributed to the better performance of OLEDs. The non-doped OLEDs showed NIR emission peaking at 702 nm with a maximum EQE of 1.2%. This work demonstrated that the cyano group could be used as a co-acceptor in the preparation of D–A narrowband NIR materials. In 2017, Yang *et al.* reported an HLCT-AIE emitter, **NZ2TPA** (Fig. 27), introducing a **DPA** block as a donor on the basis of **TPA-NZP** to fabricate symmetric D–π–A–π–D materials.[81] Attributed to its HLCT mechanism and AIE characteristics, **NZ2TPA** acquired an unprecedentedly high PLQY of 60% in the neat film, which was the highest among the reported organic small-molecule NIR emitters and even exceeded those of most phosphorescent NIR materials. The maximum EQE of 3.9% and an emission peak at 696 nm were achieved in the
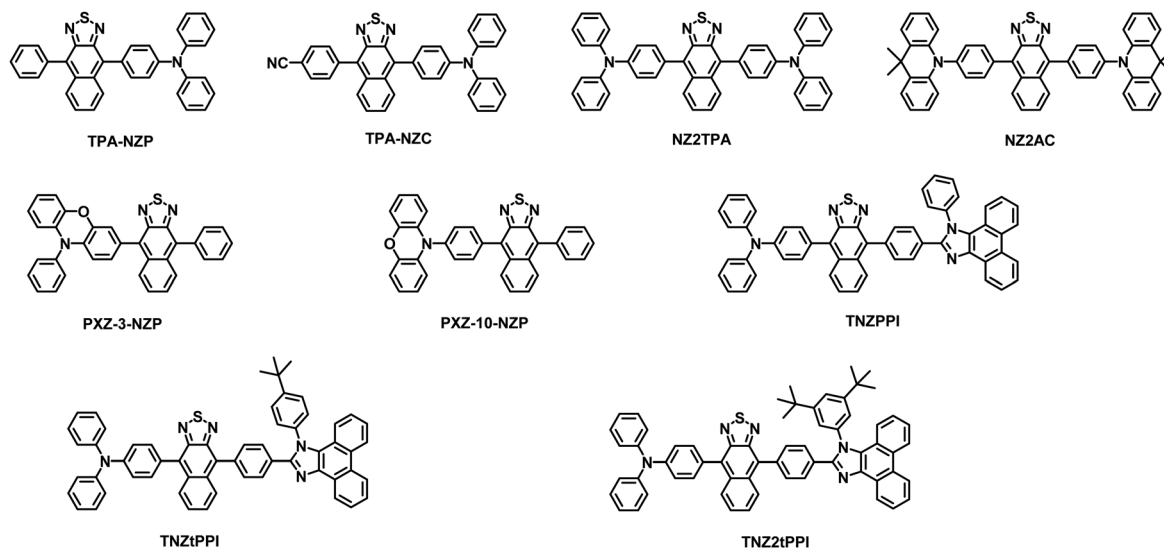
4512 | *J. Mater. Chem. C*, 2022, **10**, 4497–4520

This journal is © The Royal Society of Chemistry 2022

Fig. 27 Molecular structures of the materials containing **NZ** units.

undoped device (Fig. 28), and the brightness reached 6330 cd m^{-2}. Thanks to the HLCT mechanism, at 1000 cd m^{-2} brightness, it still showed an EQE of 2.8% with very low roll-off. This work provided a pathway for efficient D–π–A–π–D NIR OLEDs.

Subsequently, in 2017, they reported another HLCT-AIE material, **NZ2AC** (Fig. 27), also with a D–π–A–π–D structure by replacing the donor of **NZ2TPA** with **DMAC**.[82] The **NZ2AC**-based doped device achieved a maximum EQE of 6.2% with an emission peak at 612 nm. Due to the AIE properties of **NZ2AC**, the non-doped OLEDs also achieved a deep red emission at 663 nm and a maximum EQE of 2.8%, corresponding to a maximum EUE of 93%. Because of the simultaneous HLCT and AIE features, both the doped and non-doped devices exhibited low efficiency roll-offs at high brightness, with EQEs of 3.0% and 2.3% at 5000 cd m^{-2}, respectively.

Fig. 28 (a) The structures of the **NZ2TPA**-based device as well as the energy levels of the used materials. (b) EQE *versus* brightness (inset: EL spectrum at 8 V). (c) Curve of EQE *versus* brightness (inset: EL spectrum at 7 V). (d) *J–V–L* characteristics. Reproduced with permission from ref. 81. Copyright 2017 John Wiley & Sons.

In 2017, Yang *et al.* published two NIR emitters, **PXZ-3-NZP** and **PXZ-10-NZP** (Fig. 27), which were composed of donor and acceptor moieties as well as 10-substituted isomeride **PXZ-10-NZP** for the purpose of comparison and understanding the essential difference of their excited state properties.[83] As a comparison, **PXZ-10-NZP** showed a far inferior performance to that of **PXZ-3-NZP** in both non-doped and doped devices, due to the instinct CT character of its S$_1$ excited state. The EL peak of the undoped device was located at 738 nm and the maximum EQE was 0.82%. The wavelength of this undoped device was one of the records of NIR fluorescent materials.

High-efficiency organic deep red/NIR emitters with desirable PLQYs and satisfactory EUE were still limited. In 2019, Tang and co-workers prepared three deep red/NIR D–A–D* emitters, **TNZPPI**, **TNZtPPI** and **TNZ2tPPI**, by using **PPI/TPA** as the asymmetric donor and **NZ** as the acceptor. The *tert*-butyl was introduced to regulate the molecular interactions.[73] Their interesting characterization of hybrid excited states containing tuned local excited and CT components was confirmed, and the effective high-lying RISC channel could be activated because of their large T$_2$–T$_1$ energy gap and small T$_4$–S$_2$ energy splitting, which matched well with the hot exciton mechanism. Among them, the doped device based on **TNZPPI** displayed the best performance with a deep red emission of 648 nm, a maximum EQE of 6.83% and an EUE of 82%. The electronic effect of the molecule structure and intermolecular interactions were all relative to their performance, which is very important for the design of high-efficiency **NZ**-based OLED materials.
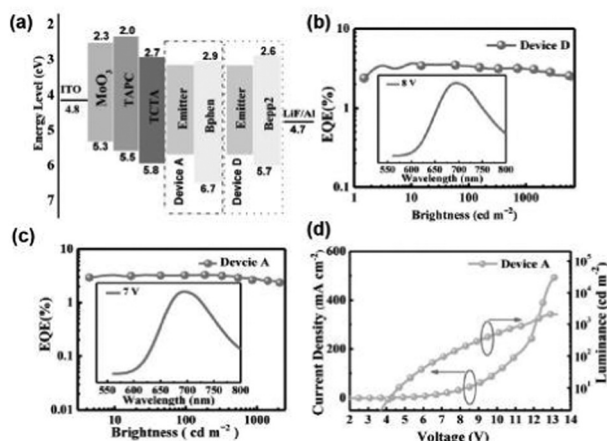
2.4 PTZ based emitters

PTZ, as a classical electron-rich group, was first used in dye-sensitized solar cells.[84,85] **It** has been widely applied as an electron donor for the construction of efficient organic light emitting materials.[36,58] A large number of **PTZ**-based derivatives show multiple molecular conformations, leading to different aggregation states and intermolecular interactions
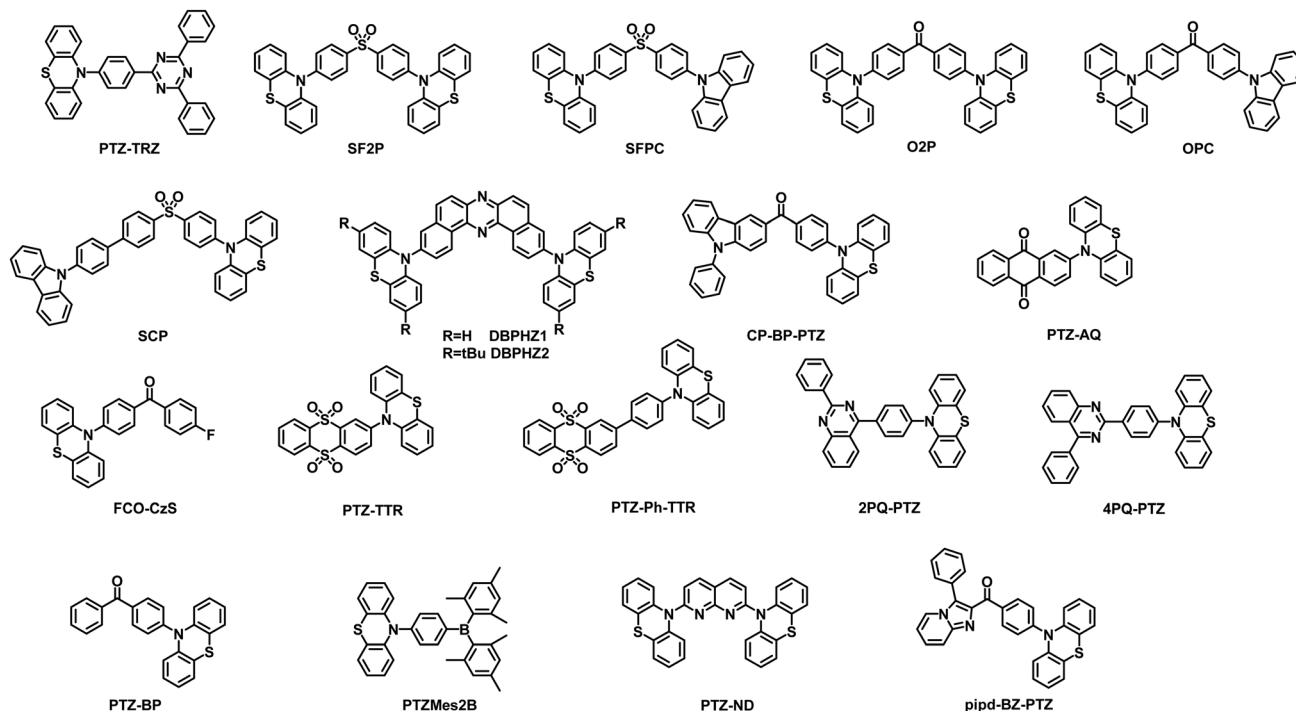
This journal is © The Royal Society of Chemistry 2022

J. Mater. Chem. C, 2022, **10**, 4497–4520 | **4513**

Fig. 29 Molecular structures of the materials containing **PTZ** units.

in the solid state. These features also entitle **PTZ**-based derivatives with some interesting characteristics such as AIE activity, piezochromic properties, *etc.*

In 2014, Adachi *et al.* developed a material, **PTZ-TRZ** (Fig. 29), containing the **PTZ** donor unit and 2,4,6-triphenyl-1,3,5-triazine (**TRZ**), the acceptor unit, which exhibited TADF properties.[86] Resulting from the distortion of **PTZ**, there existed two ground-state conformers with different energy gaps between the S_1 and T_1 states (1.14 and 0.18 eV). The PL spectra of **PTZ-TRZ** in toluene showed two broad, structureless emissions, which were attributed to intramolecular charge-transfer fluorescence from the quasi-axial conformation and quasi-equatorial conformation of **PTZ** (Fig. 30), respectively. The maximum EQE of the doped OLED based on **PTZ-TRZ** reached 10% with dual ICT fluorescence. The work reconfirmed the importance of structural chemical control in TADF materials. In 2018, Chou *et al.* reinvestigated the photophysical properties of **PTZ-TRZ**.[87] They explained that the complicated excitation behavior in toluene, in part, was due to the UV absorption cut-off region for toluene where the <315 nm excitation was greatly distorted by solvent absorption. Switching the solvent to cyclohexane with the UV cut-off wavelength at 235 nm simplified the results. In cyclohexane, quasi-axial and quasi-equatorial conformers existed for **PTZ-TRZ** in the ground state (Fig. 31). Upon electronic excitation, both conformers underwent structural relaxation to an energy minimum state where the **PTZ** was in a planar configuration.

In 2014, in order to solve the serious roll-off problem in the solid state, Chi *et al.* designed two TADF compounds SF2P and SFPC (Fig. 29), using **DPS** as the acceptor part, and **PTZ** and **Cz** as the donor, respectively.[88] **SFPC** exhibited artful packing and
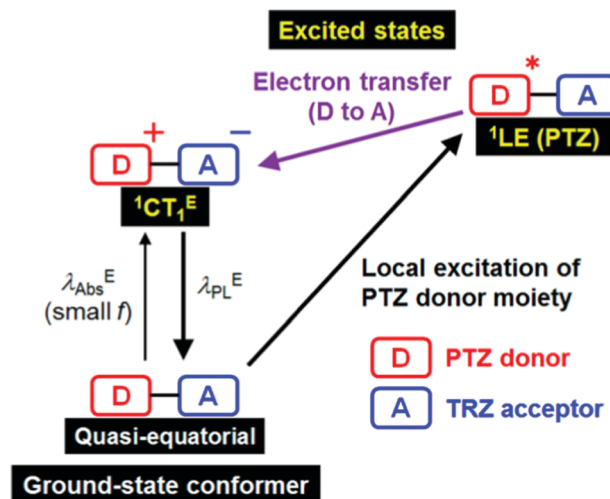

Fig. 30 Schematic diagram of the one indirect excitation pathway of λE_{PLs} of **PTZ-TRZ**. Reproduced with permission from ref. 86. Copyright 2014 American Chemical Society.

highly ordered alignment without any π–π interactions, providing a high delayed fluorescence PLQY value of 93.3% in the solid state. The ΔE_{ST} values of **SF2P** and **SFPC** were estimated to be 0.03 eV and 0.20 eV, respectively. At the same time, **SFPC** could also show strong ML without treatment. Thus, exploiting a design and synthetic strategy to integrate the features of TADF, AIE, and ML into one compound was successfully achieved.

Chi *et al.* then explored another asymmetric D–A–D′ molecule similar to **SFPC**, **OPC** (Fig. 29), whose acceptor part was replaced

4514 | *J. Mater. Chem. C*, 2022, **10**, 4497–4520

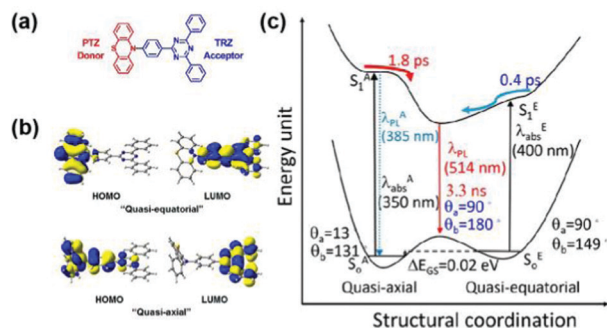This journal is © The Royal Society of Chemistry 2022

Fig. 31 (a) Molecular structures. (b) HOMO and LUMO of the ground-state quasi-equatorial and quasi-axial conformers of **PTZ-TRZ** calculated at the CAM-B3LYP/cc-pVDZ level, respectively. (c) Schematic energy level diagram of **PTZ-TRZ** in cyclohexane solution exhibiting excited-state structural relaxation. Reproduced with permission from ref. 86. Copyright 2014 American Chemical Society and ref. 87. Copyright 2018 American Chemical Society.

by **DPS** with benzophenone.[89] **OPC** was derived from two parent molecules, dicarbazolyl-substituted benzophenone (**O2C**)[90] and diphenothiazinyl-substituted benzophenone (**O2P**)[91] with inherited emission from **O2C** and **O2P** (Fig. 29). Delayed fluorescence at 580 nm of **OPC** was confirmed according to temperature dependence measurements (Fig. 32). This finding provided a feasible molecular strategy to design AIDF white light-emitting organic molecules.

Chi et al. continually explored the dual-emissive compound, **SCP** (Fig. 29), according to the same design principle.[92] **SCP** exhibited remarkable and linearly tunable mechanochromism and bright white-light emission with TADF character by fully inheriting the photophysical properties of the parent molecules **SC2** and **SP2**. The PL spectrum showed the deep blue emission at 415 nm from **SC2** and the yellow-green emission at 545 nm from **SP2**, respectively (Fig. 33). These observations demonstrated that creating asymmetric molecules following the principle of molecular heredity holds promise as a strategy for the development of functional materials.

In 2017, on the basis of **POZ-DBPHZ**,[93] Takeda et al. developed U-shaped (D–A–D) conjugated multi-functional molecules, **DBPHZ1** and **DBPHZ2** (Fig. 29), comprising **DBPHZ** as an acceptor and **PTZ** as a donor.[94] **DBPHZ1** and **DBPHZ2** showed a significant response to a variety of external stimuli because of the "two-conformation-switchable" **PTZ** units. Time-resolved photophysical measurements revealed that **DBPHZ1** possessed a very small ΔE_{ST} induced by efficient HOMO/LUMO decoupling and exhibited strong TADF. Finally, the doped device based on **DBPHZ1** achieved a maximum EQE of 16.8% with an electroluminescent peak at 613 nm.

For TADF-based OLEDs, the problem of serious efficiency roll-off at high brightness is an obstacle for their commercialization. The intermolecular electron-exchange interaction, as described by Dexter energy transfer (DET), dominates the concentration quenching of DF molecules.[95] Owing to the short-range nature of DET, high-concentration exciton annihilation can be effectively relieved in loosely aligned luminogenic
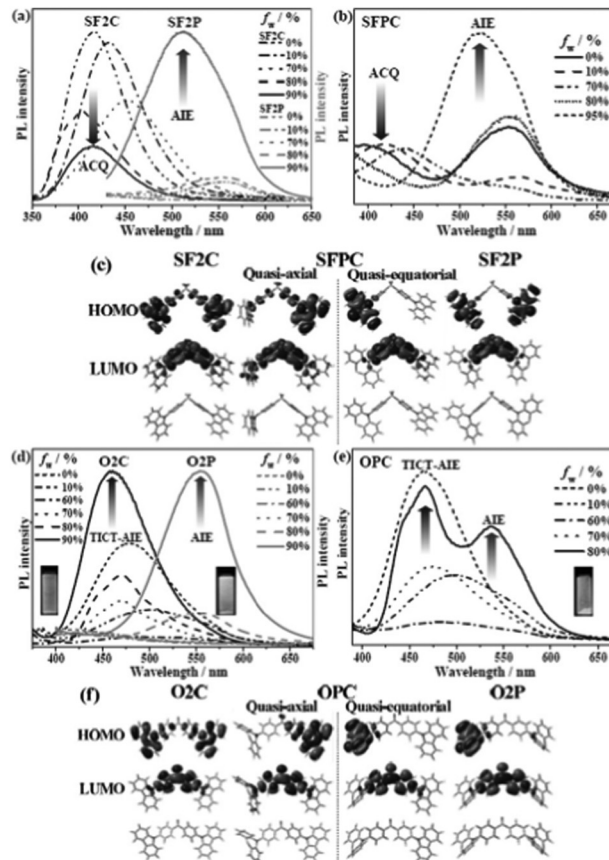

Fig. 32 PL spectra of **SF2C** and **SF2P** (a), **SFPC** (b), **O2C** and **O2P** (d), and **OPC** (e) in THF/water mixtures with different f_w. The HOMO, LUMO, and conformations of **SF2P**, **SFPC**, and **SF2C** (c), and **O2C**, **O2P**, and **OPC** (f) were optimized and calculated at B3LYP/6-31G(d,p). Reproduced with permission from ref. 89. Copyright 2015 John Wiley & Sons.

molecules with weak intermolecular interactions. In recent years, the AIDF materials have shown the potential to provide a possible solution to reduce the efficiency roll-off. Based on this concept, Tang et al. designed and synthesized three compounds, **CP-BP-PXZ**, **CP-BP-PTZ** (Fig. 29) and **CP-BP-DMAC**.[41] All of them showed obvious AIE characteristics, with PLQYs of 58%, 45.3% and 67.4% in neat films, respectively. The undoped **CP-BP-PTZ** device displayed a heavy efficiency roll-off which might be due to the unbalanced charge transport of **CP-BP-PTZ** as inferred from the current density–voltage curves of its pure hole- and electron-only devices. The non-doped OLEDs of these AIDF materials provided lower turn-on voltages and higher brightness than doped devices. Significantly high CE, PE and EQE up to 59.1 cd A^{-1} and 65.7 lm W^{-1} and 18.4% were obtained in **CP-BP-PXZ** undoped devices, comparable to doped devices. The non-doped devices showed the obvious merit of smaller efficiency roll-off compared with the doped ones.

Subsequently, in 2018, Tang et al. published another molecule **PTZ-AQ** (Fig. 29) which exhibited polymorphism, AIE, MCL, and TADF characteristics.[96] By controlling the precipitation conditions, five different aggregates were obtained with emission from green to deep red (Fig. 34). Among them,

This journal is © The Royal Society of Chemistry 2022

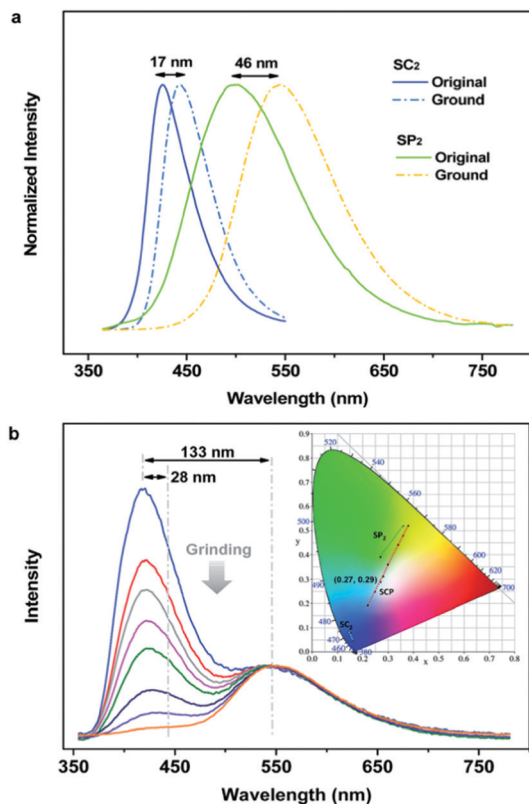J. Mater. Chem. C, 2022, **10**, 4497–4520 | **4515**

Fig. 33 (a) PL spectra of **SC2** and **SP2** in the solid state. (b) Changes of PL spectra of **SCP** under grinding.

the R-crystal exhibited considerable TADF properties, with a high PLQY of 84.8% and a small ΔE_{ST} of 0.01 eV. This work further provided the possibility of achieving multifunctional OLED materials. Li's group reported an ML **PTZ** derivative of **FCO-CzS** (Fig. 29), in which the D–A structure further enhanced the dynamic electronic properties and the fluorine atom increased the intermolecular interactions and restricted non-radiative transitions, promoting PL and ML emissions.[97] **FCO-CzS** showed AIE activity and variable mechanical luminescence

ranging from blue to white and yellow under continuous mechanical stimulation. The single crystal structure analysis and theoretical calculations as well as the comparison with **FCO-CzO** indicated that the source of dynamic mechanical luminescence was related to the multiple conformations of **PTZ**. This finding revealed the close relationship between the molecular conformation and ML process, which further deepened the understanding about the ML properties of **PTZ** derivatives.

PTZ exhibits dual stable conformations universally and showed the probability of exhibiting dual emissions during excitation, suggesting its great potential in the development of single emitters for highly efficient WOLEDs. In 2018, Li and colleagues proposed a series of single white emitters to simplify the device structure.[98] Four emitters **PTZ-TTR**, **PTZ-Ph-TTR** (Fig. 29), **DMAC-TTR**, and **DMAC-Ph-TTR** which could theoretically exhibit dual stable conformations and TADF characteristics were achieved. Two emission peaks were observed in their PL spectra deriving from quasi-axial conformation and quasi-equatorial conformation. Their band gaps and relative distributions could be well adjusted by changing the donor moieties with different flexibilities. The relative distribution of dual conformations could also be well tuned by controlling the interaction between the donor and acceptor segments. Through careful optimization, the **PTZ-TTR** based WOLEDs exhibited standard white light emission with CIE coordinates of (0.33, 0.33) and a high CRI value of 92. The device based on **PTZ-Ph-TTR** achieved an emission close to that of warm white light and a high maximum forward-viewing EQE of 16.34% (Fig. 35).

In 2020, Zhang *et al.* reported two single white emitters, **2PQ-PTZ** and **4PQ-PTZ** (Fig. 29), considering the distinct advantages of **PTZ** conformation isomers.[99] Two distinct emission bands from the quasi-axial and quasi-equatorial conformation isomers of **PTZ** were observed in both **2PQ-PTZ** and **4PQ-PTZ** in dilute
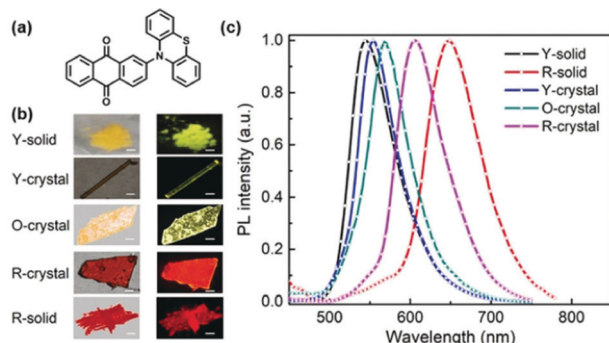

Fig. 34 (a) The molecular structure of **PTZ-AQ**. (b) Photographs of the five solid states of **PTZ-AQ** (left: under ambient light; right: under UV excitation; scale bar: 200 mm). (c) PL spectra of **PTZ-AQ** in different aggregation states. Reproduced with permission from ref. 96. Copyright 2018 John Wiley & Sons.
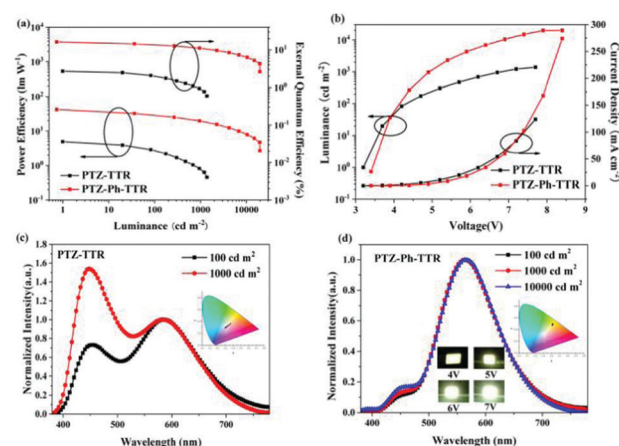
Fig. 35 (a) PE-luminance-EQE curves of **PTZ-TTR** and **PTZ-Ph-TTR**. (b) Luminance−voltage−current density curves and normalized EL spectra of **PTZ-TTR** and **PTZ-Ph-TTR**. (c) Normalized EL spectra of **PTZ-TTR** (inset): CIE variations from 100 to 1000 cd m^{-2}. (d) Normalized EL spectra of **PTZ-Ph-TTR** (inset: CIE variations from 100 to 10000 cd m^{-2} and observed emissions under different driving voltages)-based WOLEDs. Reproduced with permission from ref. 98. Copyright 2018 American Chemical Society.

4516 | *J. Mater. Chem. C*, 2022, **10**, 4497–4520

This journal is © The Royal Society of Chemistry 2022

solutions of 10^{-4} M toluene. According to X-ray crystallography analysis, **2PQ-PTZ** possessed a pair of quasi-axial and quasi-equatorial isomers with an accurate molar ratio of 1 : 1. A **2PQ-PTZ**-based WOLED with CIE coordinates of (0.32, 0.34) and color rendering index (CRI) of 89 was demonstrated. The WOLEDs exhibited a high EQE of 10.12% at a lower doping ratio of 1 wt%. With the increase of doping ratio to 18%, a record-high EQE of 25.0% in **PTZ**-based TADF OLEDs was also obtained.

With the same design strategy, in 2019, Wang et al. reported an organic molecule **PTZ-BP** (Fig. 29) consisting of a **PTZ** donor and a **BP** acceptor.[100] The PL spectra of **PTZ-BP** in diluted toluene solution at room temperature and low temperature showed two maximum emission values at 440 nm and 550 nm, respectively, and the emission at 550 nm showed typical TADF characteristics. The X-ray structure of the single crystal and PL spectra showed that the two emission peaks were derived from the H-extra and H-intra conformations of **PTZ-BP,** respectively. The doped OLEDs based on the 5,5′-di(9H-carbazol-9-yl)-3,3′-bipyridine (DczDPy, Fig. 20): **PTZ-BP** system showed good properties with a maximum EQE of 6.2%. Furthermore, they also used CBP instead of DczDPy as a host to fabricate an EL device with the same device scheme. The device with the **PTZ-BP**:CBP-doped film (4 wt%) as the emitter layer showed a maximum CE of 15.5 cd A^{-1} and an EQE of 5.44%, respectively.

As mentioned above, it is an effective solution to reduce the intermolecular interactions between molecules in order to achieve efficient TADF with reduced efficient roll-off. In 2019, Lu's group synthesized a TADF molecule, **PTZMes₂B** (Fig. 29), by using dimethylarylborane (Mes₂B) as a space-repelling electron acceptor and **PTZ** as a donor.[101] XRD analysis showed that the donor and acceptor were connected in a torsional way with a dihedral angle of 87.83°. The PL spectrum of the undoped film showed a PLQY of 65% and ΔE_{ST} of 0.18 eV. The maximum EQE of the undoped device based on **PTZMes₂B** was 19.66%, and the EQE could remain at 17.31% at a high luminance of 1500 cd m^{-2}.

In 2019, Chen et al. reported three TADF emitters, **DMAC-ND, PTZ-ND** (Fig. 29) and **PXZ-ND**.[102] The single crystal of **PTZ-ND** for X-ray diffraction analyses indicated that the torsion angles between the two PTZ units and the naphthalene part in **PTZ-ND** were 66.34° and 65.31°, respectively. The distorted structure inhibited the aggregation and quenching of the emitter, and the weak intermolecular interactions limited the intramolecular movement and maintained the molecular rigidity. The doped device based on **PTZ-ND** showed a green emission with a maximum CE of 40.9 cd A^{-1}, a PE of 31.4 lm W^{-1} and an EQE of 13.0%.

In 2020, they further reported three AIDF compounds, **pipd-BZ-PXZ, pipd-BZ-PTZ** (Fig. 29) and **pipd-BZ-DMAC**, where a strong electron-withdrawing group imidazo[1,2-a]pyridin-2-yl(phenyl)methanone (**pipd**) served as the electron acceptor and **PXZ**, **PTZ**, and **DMAC** functioned as electron donors.[103] Generated by a strong intramolecular CT effect, **pipd-BZ-PXZ** and **pipd-BZ-PTZ** exhibited orange to red emission in solution and neat films. The 6 wt% doped device of **pipd-BZ-PTZ** showed the best results: a maximum CE of 55.41 cd A^{-1}, a maximum PE

of 58.03 lm W^{-1} and a maximum EQE of 15.77%. At a 20 wt% doping concentration, the device performance was reduced, but the efficiency roll-off was greatly improved. This work once again demonstrated the feasibility of designing AIDF materials in achieving a low efficiency roll-off.

3. Conclusion and outlook

In summary, we have reviewed a variety of efficient sulphur-containing materials classified based on different functional groups including **DBT**, **DPS**, **BZ/NZ** and **PTZ** units. Sulphur possesses two lone pairs of electrons and can form sulfoxide or sulfone functional groups with electron-deficient characteristics. Therefore, sulphur-based fluorophores are promising materials for high-efficiency OLEDs. Their basic electronic structure, spatial structure and photophysical properties are summarized. To achieve OLEDs with excellent performance, all singlet and triplet excitons should be utilized for radiation luminescence in the device. The two main mechanisms for obtaining 100% IQE in pure organic small molecules, TADF and HLCT, have also been illustrated. **DBT** with an electron-rich nature is usually used in TADF molecules as an assistant donor and is responsible for generating π–π interactions to improve the EL properties. **DPS** derivatives are widely applied in green-blue OLEDs, mainly as an acceptor fragment of TADF materials. Several devices based on this maintain the highest level of OLED performance. **BZ** and **NZ** serve as the classical acceptors for HLCT materials, and a large number of OLEDs with good device performance, simplified device structures and small efficiency roll-offs are obtained. However, compared with TADF molecules, OLEDs based on **BZ** and **NZ** derivatives still have much room for further improvement in device efficiency. **PTZ** with multiple conformations is commonly utilized both in hot exciton and TADF materials. They also show potential applications in single-molecule based WOLEDs. These discussed sulphur-containing materials all cross the theoretical limited EQE (5%) by harvesting triplet excitons to the singlet state through RISC. Some special phenomena found in S-containing materials such as AIE and ML properties are also demonstrated. We believe that our summarization can be used to guide the choice of new sulphur-containing efficient emitters and facilitate their applications in OLEDs. Further research and the development of new sulphur-containing derivatives is ongoing to achieve breaking of the theoretical limited EQE while maintaining stable CIE color coordinates and low efficiency roll-off to elongate the operation lifetime.

Conflicts of interest

There are no conflicts to declare.

Acknowledgements

This journal is © The Royal Society of Chemistry 2022

J. Mater. Chem. C, 2022, **10**, 4497–4520 | **4517**

References

1 C. W. Tang and S. A. Van Slyke, *Appl. Phys. Lett.*, 1987, **51**, 913–915.

2 L. S. Hung and C. H. Chen, *Mater. Sci. Eng., R*, 2002, **39**, 143–222.

3 S. Reineke, *Nat. Mater.*, 2015, **14**, 459–462.

4 M. A. Baldo, D. F. O'Brien, M. E. Thompson and S. R. Forrest, *Phys. Rev. B: Condens. Matter Mater. Phys.*, 1999, **60**, 14422–14428.

5 L. Xiao, S.-J. Su, Y. Agata, H. Lan and J. Kido, *Adv. Mater.*, 2009, **21**, 1271–1274.

6 K. H. Kim, C. K. Moon, J. H. Lee, S. Y. Kim and J. J. Kim, *Adv. Mater.*, 2014, **26**, 3844–3847.

7 Y. C. Zhu, L. Zhou, H. Y. Li, Q. L. Xu, M. Y. Teng, Y. X. Zheng, J. L. Zuo, H. J. Zhang and X. Z. You, *Adv. Mater.*, 2011, **23**, 4041–4046.

8 H. Shin, S. Lee, K. H. Kim, C. K. Moon, S. J. Yoo, J. H. Lee and J. J. Kim, *Adv. Mater.*, 2014, **26**, 4730–4734.

9 K. Udagawa, H. Sasabe, C. Cai and J. Kido, *Adv. Mater.*, 2014, **26**, 5062–5066.

10 K. H. Kim, S. Lee, C. K. Moon, S. Y. Kim, Y. S. Park, J. H. Lee, J. Woo Lee, J. Huh, Y. You and J. J. Kim, *Nat. Commun.*, 2014, **5**, 4769.

11 M. A. Baldo, D. F. O'Brien, Y. You, A. Shoustikov, S. Sibley, M. E. Thompson and S. R. Forrest, *Nature*, 1998, **395**, 151–154.

12 D. Chen, W. Li, L. Gan, Z. Wang, M. Li and S.-J. Su, *Mater. Sci. Eng., R*, 2020, **142**, 100581.

13 S. Sinha and A. P. Monkman, *Appl. Phys. Lett.*, 2003, **82**, 4651–4653.

14 S. Sinha, C. Rothe, R. Guntner, U. Scherf and A. P. Monkman, *Phys. Rev. Lett.*, 2003, **90**, 127402.

15 C.-J. Chiang, A. Kimyonok, M. K. Etherington, G. C. Griffiths, V. Jankus, F. Turksoy and A. P. Monkman, *Adv. Funct. Mater.*, 2013, **23**, 739–746.

16 W. Li, D. Liu, F. Shen, D. Ma, Z. Wang, T. Feng, Y. Xu, B. Yang and Y. Ma, *Adv. Funct. Mater.*, 2012, **22**, 2797–2803.

17 W. Li, Y. Pan, R. Xiao, Q. Peng, S. Zhang, D. Ma, F. Li, F. Shen, Y. Wang, B. Yang and Y. Ma, *Adv. Funct. Mater.*, 2014, **24**, 1609–1614.

18 C. Lin, P. Han, S. Xiao, F. Qu, J. Yao, X. Qiao, D. Yang, Y. Dai, Q. Sun, D. Hu, A. Qin, Y. Ma, B. Z. Tang and D. Ma, *Adv. Funct. Mater.*, 2021, 2106912, DOI: 10.1002/adfm.202106912.

19 H. Kaji, H. Suzuki, T. Fukushima, K. Shizu, K. Suzuki, S. Kubo, T. Komino, H. Oiwa, F. Suzuki, A. Wakamiya, Y. Murata and C. Adachi, *Nat. Commun.*, 2015, **6**, 8476.

20 H. Tanaka, K. Shizu, H. Miyazaki and C. Adachi, *Chem. Commun.*, 2012, **48**, 11392–11394.

21 J. Jortner, S. I. Choi, J. L. Katz and S. A. Rice, *Phys. Rev. Lett.*, 1963, **11**, 323–326.

22 D. Y. Kondakov, *Philos. Trans. R. Soc., A*, 2015, **373**, 20140321.

23 H. Uoyama, K. Goushi, K. Shizu, H. Nomura and C. Adachi, *Nature*, 2012, **492**, 234–238.

24 X. Cai and S.-J. Su, *Adv. Funct. Mater.*, 2018, **28**, 1802558.

25 W.-C. Chen, C.-S. Lee and Q.-X. Tong, *J. Mater. Chem. C*, 2015, **3**, 10957–10963.

26 R. A. Keller, *Chem. Phys. Lett.*, 1969, **3**, 27–29.

27 S. Reindl and A. Penzkofer, *Chem. Phys.*, 1996, **211**, 431–439.

28 R. W. Redmond, I. E. Kochevar, M. Krieg, G. Smith and W. G. Mcgimpsey, *J. Phys. Chem. A*, 1997, **101**, 2773–2777.

29 H. Fukumura, K. Kikuchi, K. Koike and H. Kokubun, *J. Photochem. Photobiol., A*, 1988, **42**, 283–291.

30 P. T. Chou, M. L. Martinez and S. L. Studer, *J. Phys. Chem.*, 1991, **95**, 10306–10310.

31 M. L. Martinez, S. L. Studer and P. T. Chou, *J. Am. Chem. Soc.*, 1990, **112**, 2427–2429.

32 X. Qiu, Y. Xu, C. Wang, M. Hanif, J. Zhou, C. Zeng, Y. Li, Q. Jiang, R. Zhao, D. Hu and Y. Ma, *J. Mater. Chem. C*, 2019, **7**, 5461–5467.

33 J.-Y. Hu, Y.-J. Pu, F. Satoh, S. Kawata, H. Katagiri, H. Sasabe and J. Kido, *Adv. Funct. Mater.*, 2014, **24**, 2064–2071.

34 C. Li, M. Hanif, X. Li, S. Zhang, Z. Xie, L. Liu, B. Yang, S. Su and Y. Ma, *J. Mater. Chem. C*, 2016, **4**, 7478–7484.

35 W. Z. Yuan, X. Bin, G. Chen, Z. He, J. Liu, H. Ma, Q. Peng, B. Wei, Y. Gong, Y. Lu, G. He and Y. Zhang, *Adv. Opt. Mater.*, 2017, **5**, 1700466.

36 L. Yao, S. Zhang, R. Wang, W. Li, F. Shen, B. Yang and Y. Ma, *Angew. Chem., Int. Ed.*, 2014, **53**, 2119–2123.

37 H. Mutlu, E. B. Ceper, X. Li, J. Yang, W. Dong, M. M. Ozmen and P. Theato, *Macromol. Rapid Commun.*, 2019, **40**, 1800650.

38 R. A. Keller, *Chem. Phys. Lett.*, 1969, **3**, 27–29.

39 S. Reindl and A. Penzkofer, *Chem. Phys.*, 1996, **211**, 431–439.

40 R. W. Redmond, I. E. Kochevar, M. Krieg, G. Smith and W. G. Mcgimpsey, *J. Phys. Chem. A*, 1997, **101**, 2773–2777.

41 J. Huang, H. Nie, J. Zeng, Z. Zhuang, S. Gan, Y. Cai, J. Guo, S.-J. Su, Z. Zhao and B. Z. Tang, *Angew. Chem., Int. Ed.*, 2017, **56**, 12971–12976.

42 H. L. Shen, F. Huang, L. T. Hou, H. B. Wu, W. Cao, W. Yang and Y. Cao, *Synth. Met.*, 2005, **152**, 257–260.

43 J. A. Mikroyannidis, H. A. Moshopoulou, J. A. Anastasopoulos, M. M. Styllanakis, L. Fenenko and C. Adachi, *J. Polym. Sci., Part A: Polym. Chem.*, 2006, **44**, 6790–6800.

44 W. S. Huang, Y. H. Wu, Y. C. Hsu, H. C. Lin and J. T. Lin, *Polymer*, 2009, **50**, 5945–5958.

45 J. Guo, X.-L. Li, H. Nie, W. Luo, S. Gan, S. Hu, R. Hu, A. Qin, Z. Zhao, S.-J. Su and B. Z. Tang, *Adv. Funct. Mater.*, 2017, **27**, 1606458.

46 J. Fan, L. Lin and C.-K. Wang, *J. Mater. Chem. C*, 2017, **5**, 8390–8399.

47 J. Guo, X.-L. Li, H. Nie, W. Luo, R. Hu, A. Qin, Z. Zhao, S.-J. Su and B. Z. Tang, *Chem. Mater.*, 2017, **29**, 3623–3631.

48 R. Huang, N. A. Kukhta, J. S. Ward, A. Danos, A. S. Batsanov, M. R. Bryce and F. B. Dias, *J. Mater. Chem. C*, 2019, **7**, 13224–13234.

49 R. Huang, J. S. Ward, N. A. Kukhta, J. Avó, J. Gibson, T. Penfold, J. C. Lima, A. S. Batsanov, M. N. Berberan-

4518 | *J. Mater. Chem. C*, 2022, **10**, 4497–4520

This journal is © The Royal Society of Chemistry 2022

Santos, M. R. Bryce and F. B. Dias, *J. Mater. Chem. C*, 2018, **6**, 9238–9247.

50 Q. Zhang, B. Li, S. Huang, H. Nomura, H. Tanaka and C. Adachi, *Nat. Photonics*, 2014, **8**, 326–332.

51 X. Zeng, K.-C. Pan, W.-K. Lee, S. Gong, F. Ni, X. Xiao, W. Zeng, Y. Xiang, L. Zhan, Y. Zhang, C.-C. Wu and C. Yang, *J. Mater. Chem. C*, 2019, **7**, 10851–10859.

52 M. Liu, R. Komatsu, X. Cai, H. Sasabe, T. Kamata, K. Nakao, K. Liu, S.-J. Su and J. Kido, *Adv. Opt. Mater.*, 2017, **5**, 1700334.

53 Q. Zhang, J. Li, K. Shizu, S. Huang, S. Hirata, H. Miyazaki and C. Adachi, *J. Am. Chem. Soc.*, 2012, **134**, 14706–14709.

54 S. Wu, M. Aonuma, Q. Zhang, S. Huang, T. Nakagawa, K. Kuwabara and C. Adachi, *J. Mater. Chem. C*, 2014, **2**, 421–424.

55 Q. Zhang, D. Tsang, H. Kuwabara, Y. Hatae, B. Li, T. Takahashi, S. Y. Lee, T. Yasuda and C. Adachi, *Adv. Mater.*, 2015, **27**, 2096–2100.

56 L. Zhan, Z. Chen, S. Gong, Y. Xiang, F. Ni, X. Zeng, G. Xie and C. Yang, *Angew. Chem., Int. Ed.*, 2019, **58**, 17651–17655.

57 M. Liu, R. Komatsu, X. Cai, K. Hotta, S. Sato, K. Liu, D. Chen, Y. Kato, H. Sasabe, S. Ohisa, Y. Suzuri, D. Yokoyama, S.-J. Su and J. Kido, *Chem. Mater.*, 2017, **29**, 8630–8636.

58 Z. Yang, Z. Mao, C. Xu, X. Chen, J. Zhao, Z. Yang, Y. Zhang, W. Wu, S. Jiao, Y. Liu, M. P. Aldred and Z. Chi, *Chem. Sci.*, 2019, **10**, 8129–8134.

59 M. Liu, Y. Seino, D. Chen, S. Inomata, S. J. Su, H. Sasabe and J. Kido, *Chem. Commun.*, 2015, **51**, 16353–16356.

60 X. Tang, Q. Bai, Q. Peng, Y. Gao, J. Li, Y. Liu, L. Yao, P. Lu, B. Yang and Y. Ma, *Chem. Mater.*, 2015, **27**, 7050–7057.

61 C. Fu, S. Luo, Z. Li, X. Ai, Z. Pang, C. Li, K. Chen, L. Zhou, F. Li, Y. Huang and Z. Lu, *Chem. Commun.*, 2019, **55**, 6317–6320.

62 I. Lee and J. Y. Lee, *Org. Electron.*, 2016, **29**, 160–164.

63 Y. Luo, S. Li, Y. Zhao, C. Li, Z. Pang, Y. Huang, M. Yang, L. Zhou, X. Zheng, X. Pu and Z. Lu, *Adv. Mater.*, 2020, **32**, 2001248.

64 F. B. Dias, K. N. Bourdakos, V. Jankus, K. C. Moss, K. T. Kamtekar, V. Bhalla, J. Santos, M. R. Bryce and A. P. Monkman, *Adv. Mater.*, 2013, **25**, 3707–3714.

65 X. He, T. Shan, X. Tang, Y. Gao, J. Li, B. Yang and P. Lu, *J. Mater. Chem. C*, 2016, **4**, 10205–10208.

66 H. Wang, L. Xie, Q. Peng, L. Meng, Y. Wang, Y. Yi and P. Wang, *Adv. Mater.*, 2014, **26**, 5198–5204.

67 L. Xie, G. Han, Y. Chen, H. Wang, X. Kong, X. Wei, J. Liu, Y. Yi, B. Chen, P. Wang and Y. Wang, *J. Mater. Chem. C*, 2016, **4**, 10776–10780.

68 X. Wei, Y. Chen, R. Duan, J. Liu, R. Wang, Y. Liu, Z. Li, Y. Yi, Y. Yamada-Takamura, P. Wang and Y. Wang, *J. Mater. Chem. C*, 2017, **5**, 12077–12084.

69 X. Wei, Z. Li, T. Hu, R. Duan, J. Liu, R. Wang, Y. Liu, X. Hu, Y. Yi, P. Wang and Y. Wang, *Adv. Opt. Mater.*, 2019, **7**, 1801767.

70 S. P. Xiang, Z. Huang, S. Q. Sun, X. L. Lv, L. W. Fan, S. F. Ye, H. T. Chen, R. D. Guo and L. Wang, *J. Mater. Chem. C*, 2018, **6**, 11436–11443.

71 J. Rao, C. Zhao, Y. Wang, K. Bai, S. Wang, J. Ding and L. Wang, *ACS Omega*, 2019, **4**, 1861–1867.

72 Y. P. Jeon, B. K. Kong, E. J. Lee, K.-H. Yoo and T. W. Kim, *Nano Energy*, 2019, **59**, 560–568.

73 Q. Wan, J. Tong, B. Zhang, Y. Li, Z. Wang and B. Z. Tang, *Adv. Opt. Mater.*, 2019, **8**, 1901520.

74 W. Li, Y. Pan, L. Yao, H. Liu, S. Zhang, C. Wang, F. Shen, P. Lu, B. Yang and Y. Ma, *Adv. Opt. Mater.*, 2014, **2**, 892–901.

75 C. Wang, X. Li, Y. Pan, S. Zhang, L. Yao, Q. Bai, W. Li, P. Lu, B. Yang, S. Su and Y. Ma, *ACS Appl. Mater. Interfaces*, 2016, **8**, 3041–3049.

76 J. Liu, Z. Li, T. Hu, X. Wei, R. Wang, X. Hu, Y. Liu, Y. Yi, Y. Yamada-Takamura, Y. Wang and P. Wang, *Adv. Opt. Mater.*, 2019, **7**, 1801190.

77 W. Xie, B. Li, X. Cai, M. Li, Z. Qiao, X. Tang, K. Liu, C. Gu, Y. Ma and S. J. Su, *Front. Chem.*, 2019, **7**, 276.

78 X. Chen, Z. Yang, W. Li, Z. Mao, J. Zhao, Y. Zhang, Y. C. Wu, S. Jiao, Y. Liu and Z. Chi, *ACS Appl. Mater. Interfaces*, 2019, **11**, 39026–39034.

79 W. Li, Y. Pan, R. Xiao, Q. Peng, S. Zhang, D. Ma, F. Li, F. Shen, Y. Wang, B. Yang and Y. Ma, *Adv. Funct. Mater.*, 2014, **24**, 1609–1614.

80 X. Tang, X.-L. Li, H. Liu, Y. Gao, Y. Shen, S. Zhang, P. Lu, B. Yang, S.-J. Su and Y. Ma, *Dyes Pigm.*, 2018, **149**, 430–436.

81 T. Liu, L. Zhu, C. Zhong, G. Xie, S. Gong, J. Fang, D. Ma and C. Yang, *Adv. Funct. Mater.*, 2017, **27**, 1606384.

82 T. Liu, L. Zhu, S. Gong, C. Zhong, G. Xie, E. Mao, J. Fang, D. Ma and C. Yang, *Adv. Opt. Mater.*, 2017, **5**, 1700145.

83 C. Wang, X.-L. Li, Y. Gao, L. Wang, S. Zhang, L. Zhao, P. Lu, B. Yang, S.-J. Su and Y. Ma, *Adv. Opt. Mater.*, 2017, **5**, 1700441.

84 H. N. Tian, X. C. Yang, R. K. Chen, Y. Z. Pan, L. Li, A. Hagfeldt and L. C. Sun, *Chem. Commun.*, 2007, 3741–3743, DOI: 10.1039/b707485a.

85 Z. Xie, A. Midya, K. P. Loh, S. Adams, D. J. Blackwood, J. Wang, X. Zhang and Z. Chen, *Prog. Photovoltaics*, 2010, **18**, 573–581.

86 H. Tanaka, K. Shizu, H. Nakanotani and C. Adachi, *J. Phys. Chem. C*, 2014, **118**, 15985–15994.

87 D.-G. Chen, T.-C. Lin, Y.-A. Chen, Y.-H. Chen, T.-C. Lin, Y.-T. Chen and P.-T. Chou, *J. Phys. Chem. C*, 2018, **122**, 12215–12221.

88 S. Xu, T. Liu, Y. Mu, Y. F. Wang, Z. Chi, C. C. Lo, S. Liu, Y. Zhang, A. Lien and J. Xu, *Angew. Chem., Int. Ed.*, 2015, **54**, 874–878.

89 Z. Xie, C. Chen, S. Xu, J. Li, Y. Zhang, S. Liu, J. Xu and Z. Chi, *Angew. Chem., Int. Ed.*, 2015, **54**, 7181–7184.

90 S. Y. Lee, T. Yasuda, Y. S. Yang, Q. Zhang and C. Adachi, *Angew. Chem., Int. Ed.*, 2014, **53**, 6402–6406.

91 C. J. Chen, J. Y. Liao, Z. G. Chi, B. J. Xu, X. Q. Zhang, D. B. Kuang, Y. Zhang, S. W. Liu and J. R. Xu, *J. Mater. Chem.*, 2012, **22**, 8994–9005.

92 B. Xu, Y. Mu, Z. Mao, Z. Xie, H. Wu, Y. Zhang, C. Jin, Z. Chi, S. Liu, J. Xu, Y.-C. Wu, P.-Y. Lu, A. Lien and M. R. Bryce, *Chem. Sci.*, 2016, **7**, 2201–2206.

This journal is © The Royal Society of Chemistry 2022

J. Mater. Chem. C, 2022, **10**, 4497–4520 | **4519**

93 P. Data, P. Pander, M. Okazaki, Y. Takeda, S. Minakata and
    A. P. Monkman, *Angew. Chem., Int. Ed.*, 2016, **55**, 5739–5744.

94 M. Okazaki, Y. Takeda, P. Data, P. Pander,
    H. Higginbotham, A. P. Monkman and S. Minakata, *Chem.
    Sci.*, 2017, **8**, 2677–2686.

95 J. Lee, N. Aizawa, M. Numata, C. Adachi and T. Yasuda,
    Adv. Mater., 2017, **29**, 1604856.

96 B. Huang, W. C. Chen, Z. Li, J. Zhang, W. Zhao, Y. Feng,
    B. Z. Tang and C. S. Lee, *Angew. Chem., Int. Ed.*, 2018, **57**,
    12473–12477.

97 J. Yang, J. Qin, P. Geng, J. Wang, M. Fang and Z. Li, *Angew.
    Chem., Int. Ed.*, 2018, **57**, 14174–14178.

98 K. Wang, Y.-Z. Shi, C.-J. Zheng, W. Liu, K. Liang, X. Li,
    M. Zhang, H. Lin, S.-L. Tao, C.-S. Lee, X.-M. Ou and

    X.-H. Zhang, *ACS Appl. Mater. Interfaces*, 2018, **10**,
    31515–31525.

99 B. Li, Z. Li, F. Guo, J. Song, X. Jiang, Y. Wang, S. Gao,
    J. Wang, X. Pang and L. Zhao, *ACS Appl. Mater. Interfaces*,
    2020, **12**, 14233–14243.

100 C. Li, J. Liang, B. Liang, Z. Li, Z. Cheng, G. Yang and
    Y. Wang, *Adv. Opt. Mater.*, 2019, **7**, 1801667.

101 X. Tang, Y. Tao, H. Liu, F. Liu, X. He, Q. Peng, J. Li and
    P. Lu, *Front. Chem.*, 2019, **7**, 373.

102 C. Chen, H.-Y. Lu, Y.-F. Wang, M. Li, Y.-F. Shen and
    C.-F. Chen, *J. Mater. Chem. C*, 2019, **7**, 4673–4680.

103 Z. Yang, Y. Zhan, Z. Qiu, J. Zeng, J. Guo, S. Hu, Z. Zhao,
    X. Li, S. Ji, Y. Huo and S.-J. Su, *ACS Appl. Mater. Interfaces*,
    2020, **12**, 29528–29539.